Check for updates

ADVANCED ENERGY MATERIALS
www.advenergymat.de

Weakly Solvating Electrolytes for Lithium and Post-Lithium Rechargeable Batteries: Progress and Outlook

Xue Li, Fei Luo, Naigen Zhou, Henry Adenusi, Shan Fang, Fanglin Wu,* and Stefano Passerini**

In the rapidly evolving global landscape of renewable energy sources, there is an increasing demand for high-energy-density rechargeable batteries essential for energy storage. Simultaneously, there is a growing emphasis on developing high-stability electrolytes. The concepts of high concentration electrolytes (HCEs) and localized high concentration electrolytes (LHCEs) have emerged, with notable progress achieved by altering cation-solvent and cation–anion solvation coordination environments. However, challenges persist, including high costs and low ionic conductivity. A recent development is the introduction of the weakly solvating electrolyte (WSE), which offers a new perspective on the design of stable electrolytes at conventional or low concentrations. This approach enables high-performance rechargeable batteries by modulating the coordination structure of electrolytes to generate a unique anion-driven interphase reaction chemistry. This review outlines the design principles of WSEs and their operating mechanisms when applied to rechargeable lithium and post-lithium batteries. An outlook is also presented on the future research directions of WSE, coupled with an analysis of the technological challenges.

1. Introduction

In response to the international calls for "green technologies", batteries have flourished, reaping extensive attention from both research and industrial sectors. Due to their environmental friendliness and high efficiency, rechargeable batteries have been widely adopted in electric vehicles, unmanned aerial vehicles, and portable electronic products as effective energy storage devices.[1,2] However, the energy density and charging time of commercial rechargeable batteries are not sufficient to cope with the continuous expansion of the application market.[3–5] Each component of rechargeable batteries, including positive/negative electrode, electrolyte, and so forth, must be optimized to achieve higher energy density, stability, and safety, wider operative temperature range, and longer cycle life.[6,7] Among the electrochemically active battery components, the electrolyte, as the connection between cathode and anode, should not be neglected. Compared with the advancements of the positive (cathode) and negative (anode) electrode materials, which are now at the bottleneck, the exploration of liquid electrolyte is frequently seen as a "shortcut" with a very large flexibility. In fact, the formulation of an electrolyte is faster than that of an electrode material, and its composition can be altered, taking advantage of the enormous variety of organic compounds. This is important because the formation of effective electrode/electrolyte interphases results from the electrolyte supplying the building blocks for the solid electrolyte interphase (SEI)

X. Li, F. Luo, N. Zhou, S. Fang
School of Physics and Materials Science
Nanchang University
Nanchang, Jiangxi 330031, China
E-mail: fangshan@ncu.edu.cn

H. Adenusi
Department of Science and Engineering of Matter
Environment and Urban Planning
Marche Polytechnic University
Ancona 60131, Italy

The ORCID identification number(s) for the author(s) of this article can be found under https://doi.org/10.1002/aenm.202501272

© 2025 The Author(s). Advanced Energy Materials published by Wiley-VCH GmbH. This is an open access article under the terms of the Creative Commons Attribution License, which permits use, distribution and reproduction in any medium, provided the original work is properly cited.

DOI: 10.1002/aenm.202501272

F. Wu
State Key Laboratory of Advanced Technology for Materials Synthesis and Processing
Wuhan University of Technology
Wuhan 430070, China
E-mail: fanglin-wu@whut.edu.cn

F. Wu
Hubei Key Laboratory of Fuel Cells
Wuhan University of Technology
Wuhan 430070, China

S. Passerini
Karlsruhe Institute of Technology (KIT)
Helmholtz Institute Ulm
Helmholtzstrasse 11, 89081 Ulm, Germany
E-mail: stefano.passerini@kit.edu

S. Passerini
Austrian Institute of Technology
Center for Transport Technologies
Giefinggasse 4, Vienna 1210, Austria

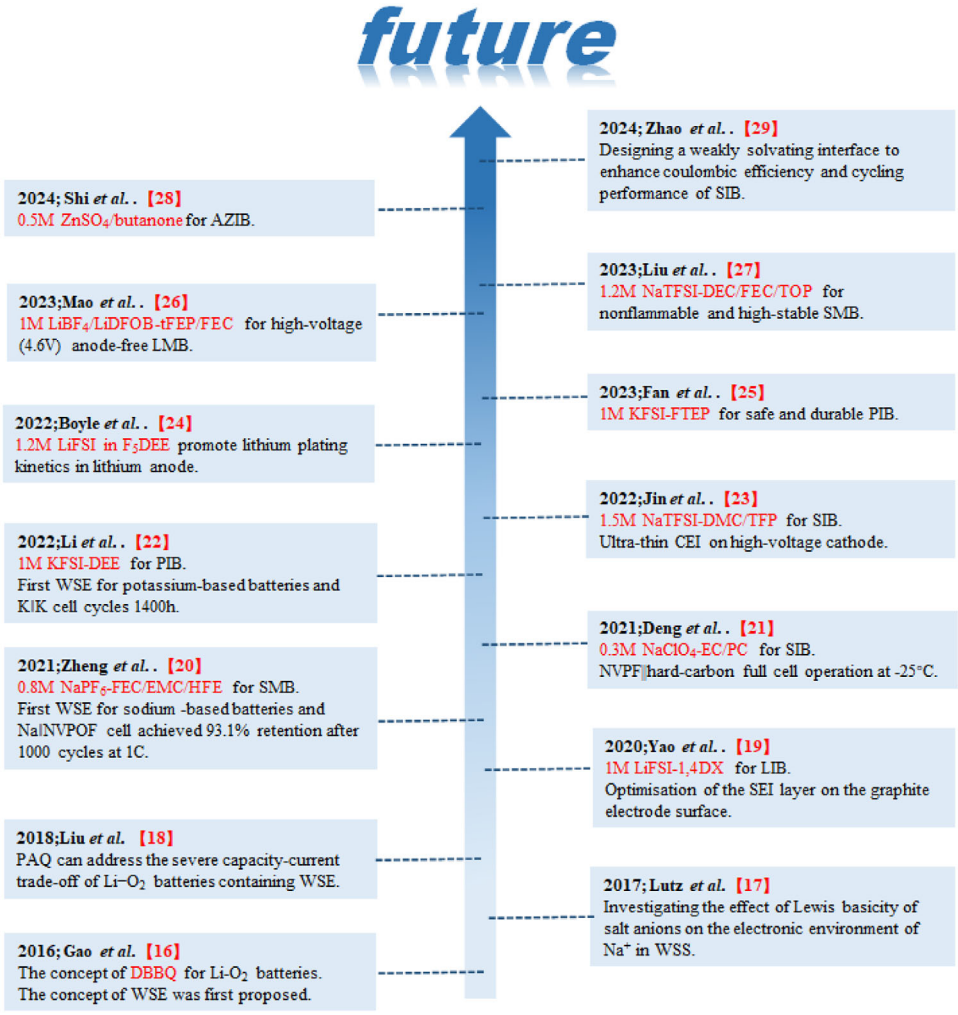

Figure 1. Schematic diagram illustrating the development of weakly solvating electrolytes for rechargeable batteries.[16–29]

at the negative electrode and cathode electrolyte interphase (CEI) at the positive electrode.[8] These interphases inhibit further electrolyte decomposition and facilitate Li^+ transport through the layer onto the electrode.[9] Currently, conventional, organic solvent-based electrolytes enable the operation of commercial Li-ion batteries (LIBs) powering our portable electronics and vehicles.

The growing activities on electrolytes for rechargeable batteries have also led to the emergence of new concepts and strategies, such as tailoring the solvation structure of the electrolyte. Recently, high concentration electrolytes (HCEs)[6,10] and localized high concentration electrolytes (LHCEs)[11,12] have been proposed and widely studied to improve the electrochemical performance of lithium metal batteries (LMBs). HCEs have been shown to enhance the interphase between the positive (or metal) electrode and the electrolyte, yielding anion-rich interphases, which provide faster lithium-ion transport.[13,14] To take advantage of such an effect while limiting the use of expensive salts, diluents have been used to form LHCEs. To preserve the local coordination of the salt-solvent clusters in HCE and, thus, favor the establishment of optimal interphases, the diluents are usually non-solvating solvents for the electrochemically active salt(s). Nonetheless, HCE and LHCE are limited by specific drawbacks, including high viscosity, poor Li^+ kinetics, and low conductivity. Additionally, they make use of highly fluorinated diluents, making them costly and hindering their practical application in LMBs.[11,15]

As a result, weakly solvating electrolytes (WSEs) are garnering interest as superior electrolytes for LMBs and post-lithium batteries: sodium, potassium, zinc, and beyond. **Figure 1** illustrates the development process of WSEs for rechargeable batteries. The solvation ability of the solvent indicates the strength of the interaction between the solvent and the electrochemically active ions (Li^+, Na^+, K^+, ...). Both the solvent and the anion can serve as ligands to coordinate with Li^+ via ion-dipole or ion-ion interactions, the solvation structure results from the anion and the solvent competition for the binding of Li^+.[30] WSEs have a unique solvation structure that differs from that of conventional electrolytes, because the use of the poorly-solvating, low dielectric constant solvent results in the anion dominating the primary solvation sheath. In this structure, abundant contact ion pairs (CIPs) and aggregates (AGGs) exist even at low and medium salt

© 2025 The Author(s). Advanced Energy Materials published by Wiley-VCH GmbH

16146840, 0, Downloaded from https://advanced.onlinelibrary.wiley.com/doi/10.1002/aenm.202501272 by Karlsruher Institut Für Technologie, Wiley Online Library on [13/05/2025]. See the Terms and Conditions (https://onlinelibrary.wiley.com/terms-and-conditions) on Wiley Online Library for rules of use; OA articles are governed by the applicable Creative Commons License

concentrations, resulting in the formation of favorable anion-rich derived anode- and cathode-electrolyte interphases (respectively, SEI and CEI). However, WSEs have yet to be extensively utilized in liquid electrolyte batteries due to the restricted solvation ability of the low dielectric constant solvents employed in WSE, which results in limited salt solubility.[11,30]

In this review, we present the design principles and the solvation structure of WSEs in relation to their functionality and physical properties, which are dependent on the type and characteristics of the weakly solvating solvents (WSS), as well as the differences with HCE and LHCE are explored. Simultaneously, we analyze the interphase modification effects of solvent-ion reaction mechanisms in WSEs on lithium batteries and assess the mechanism of action of WSEs in post-lithium battery applications. Lastly, an outlook on the development of electrolytes is provided to realize wide-temperature, long-life, and high-energy-density batteries.

2. Design Principle of WSE

2.1. Definition and Distinction of WSE from Other Electrolytes

WSE is a new type of electrolyte with its most prominent feature of weaker interactions between solvent and metal ions, and typically includes solvent molecules with lower polarity to improve battery performance. Weakly polar solvents refer to solvents with polarity between that of polar and non-polar solvents. Compared to HCE and LHCE, WSE exhibits relatively low viscosity, a reduced desolvation energy barrier, and suitable ion conductivity. Importantly, the "weak solvation force" solvents in WSE exhibit weak interactions with Li^+, reducing the coordination of solvents with Li^+ and allowing more anions to coordinate with Li^+, forming abundant CIPs and AGGs structures (**Figure 2a**).[31,32] The comparison of conventional electrolyte, HCE, LHCE, and WSE in terms of cost, viscosity, ionic conductivity, and other physical parameters is shown in Figure 2b. Compared to the CIPs and AGGs formed in HCEs and LHCEs, the solvation structure in WSEs is primarily governed by WSS. Due to the insufficient coordination capability of these solvents, anions readily enter the Li^+ solvation sheath, leading to the formation of CIPs and AGGs. The driving force here stems from the solvents' low competition for anions rather than a high salt concentration. In contrast, HCEs and LHCEs rely on bulk/localized high salt concentrations, where the limited availability of solvent molecules prevents complete salt dissociation. This forces anions to directly coordinate with Li^+—a phenomenon driven by the "crowding-out effect" of solvent molecules, wherein excessively high ion concentrations compel anions to engage in direct Li^+ contact.

2.2. Distinctive Functions of WSE

2.2.1. Enhancing the Desolvation Process

The migration of Li^+ in the battery involves four main processes: the transport of solvated Li^+ in the bulk electrolyte, the desolvation of solvated Li^+, migration of bare Li^+ within the SEI/CEI, and the diffusion of Li^+ in the electrode material.[3] The migration rate in these processes is determined by various factors, i.e., the thickness of the electrode and separator, the particle size of the active material, the electrolyte properties, and the operating temperature of the cell. The desolvation process[33] and the diffusion of Li^+ through the SEI layers are considered to be two of the most energy-consuming steps, which have a significant impact on the performance of the battery. The crucial factor in reducing the desolvation energy is to weaken the interaction between Li^+ and solvent molecules, which can be realized by WSE, leading to a substantial reduction in the energy barrier for Li^+ desolvation.[34] For example, the WSE (1M $LiBF_4$-DOL/THF) (THF: tetrahydrofuran; DOL:1,3-dioxolane) developed by Liang et al. has a lower desolvation energy barrier compared to the common commercial electrolyte (1M $LiBF_4$-PC/DME; PC: propylene carbonate; DME: dimethoxyethane) (**Figure 3a**). The dielectric constant, donor number, and steric hindrance significantly influence the interaction between Li^+ and the solvent.[35] Solvents with high dielectric constants and high donor numbers can generally dissolve and dissociate lithium salts rapidly and effectively, thereby enhancing ionic conductivity.[36] However, the solvents often exhibit strong interactions with Li^+, resulting in a complex desolvation process.[34] Compared to conventional solvents, 1,4-dioxane (1,4-DX) with an extremely low dielectric constant of 2.2 as a solvent, the activation energy for the desolvation process was reduced from 54.7 to 48.2 kJ mol^{-1}.[19] In addition, solvents with large molecular volume can lead to increased steric hindrance effect, causing increased distances between coordinating solvent molecules and cations. This weakens the interaction between solvent molecules and Li^+, which is favorable for the desolvation process, i.e., 1,2-diethoxyethane (DEE), due to its larger ethoxy groups, exhibits significantly weaker solvating ability for lithium ions compared to DME with smaller methoxy groups.[37]

2.2.2. Reduction of Solvent Polarization

In the solvent sheath of conventional electrolyte, due to the presence of electrostatic Li^+, solvent molecules are prone to polarization (Figure 3b). Solvent molecules near Li^+ carry a negative charge inside and a positive charge outside, increasing the electrophilicity of the anode region, making it easier to accept electrons and decompose on the electrode surface.[38] However, in WSE, anions participate in the solvation sheath, reducing the polarization of solvent molecules and their ability to accept electrons[39] thereby enhancing electrochemical stability. Additionally, the solvents used in WSE typically have low donor numbers and dielectric constants. A lower donor number corresponds to a weaker electron-donating capability of the solvent, which leads to diminished interactions with metal cations. This, in turn, results in a thinner solvation sheath and reduced polarization of the solvent molecules. Furthermore, a lower dielectric constant signifies reduced polarity, which also results in weaker solvent polarization.

2.2.3. Improvement of Metal Plating Kinetics

Boyle et al. proposed that the relationship between lithium deposition kinetics and solvation structure suggests that interfacial resistance has a lesser impact on the reversibility of lithium plating/stripping overpotential. Instead, the fresh lithium/electrolyte

© 2025 The Author(s). Advanced Energy Materials published by Wiley-VCH GmbH

16146840, 0, Downloaded from https://advanced.onlinelibrary.wiley.com/doi/10.1002/aenm.202501272 by Karlsruher Institut Für Technologie, Wiley Online Library on [13/05/2025]. See the Terms and Conditions (https://onlinelibrary.wiley.com/terms-and-conditions) on Wiley Online Library for rules of use; OA articles are governed by the applicable Creative Commons License

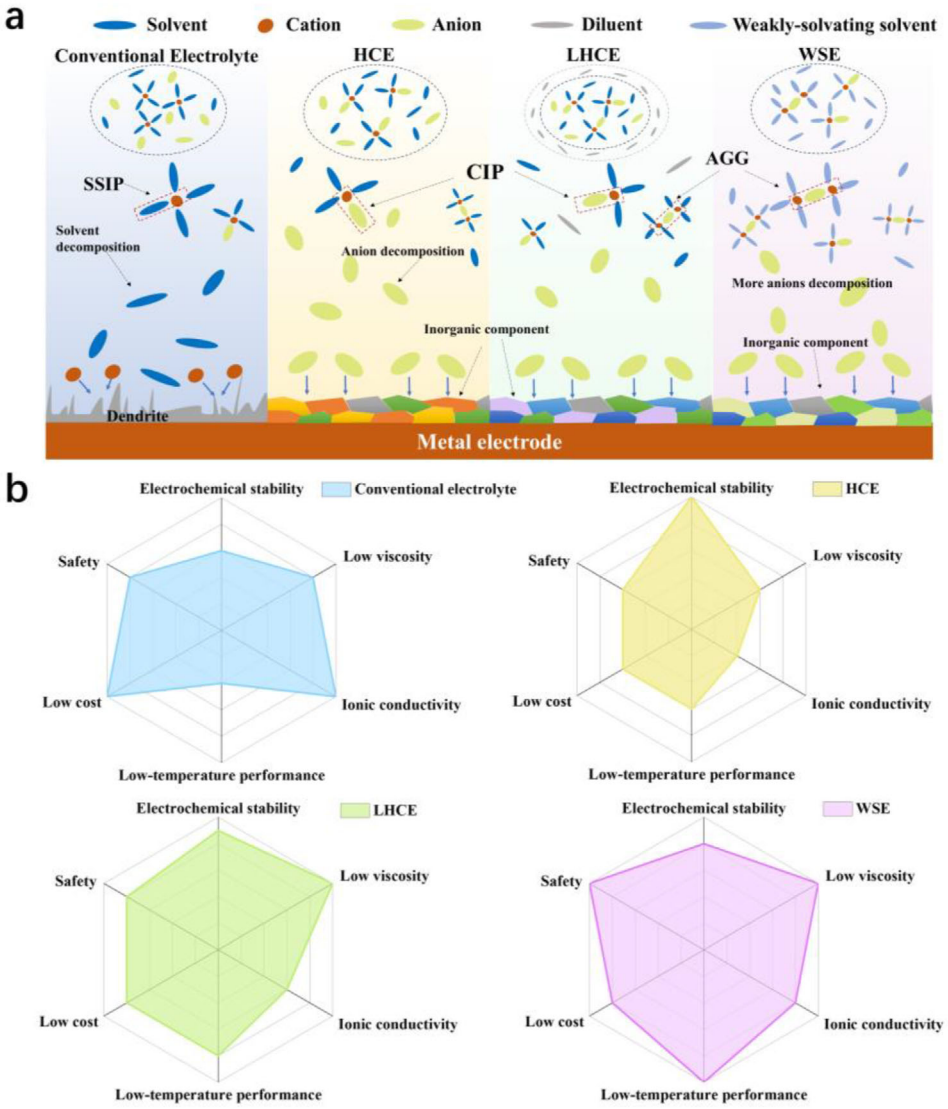

Figure 2. a) Schematic representation of salt and solvent structure (solvent separated ion pair (SSIP), contact ion pair (CIP), aggregate (AGG)) and interaction on metal electrodes in conventional electrolyte, HCE, LHCE, and WSE. b) Comparison of physical parameters of conventional electrolyte, HCE, LHCE, and WSE.

interphase has a greater influence. Additionally, the main factor affecting the uniformity of lithium deposition is not the ion diffusion rate through the SEI. Their report indicates that a weak solvation structure has a higher Li/Li$^+$ equilibrium potential and higher Li surface energy, favorable for uniform and reversible Li plating/stripping (Figure 3c).[24,40]

2.2.4. Construction of Inorganic-Rich Electrode/Electrolyte Interphase

According to Weng et al., the diffusion of Li$^+$ through the SEI film may be more critical to achieving fast kinetics than the desolvation process.[41] The decomposition of anions in WSE forms an inorganic-rich SEI/CEI layer, including Li_2CO_3, Li_2O, and LiF. Compared to traditional SEI/CEI layers, the inorganic components of the SEI/CEI layer, such as LiF and Li_3N, exhibit high mechanical strength and ionic conductivity. Their structures are more compact, uniform, and thin, which facilitates Li$^+$ transport.[42] On the anode side, an SEI rich in inorganic components can lower the energy barrier for Li$^+$ transport, suppress lithium dendrite growth and side reactions, and prohibit side reactions in the battery; on the cathode side, the inorganic components in the CEI help to restrain the dissolution of active elements and gas release. Therefore, choosing solvents with weak solvation capabilities can ameliorate the solvation structure of Li$^+$, accelerating the desolvation processes and producing uniform Li deposition morphology (Figure 3d),[43] improving the safety and lifespan of batteries.

© 2025 The Author(s). Advanced Energy Materials published by Wiley-VCH GmbH

16146840, 0, Downloaded from https://advanced.onlinelibrary.wiley.com/doi/10.1002/aenm.202501272 by Karlsruher Institut Für Technologie, Wiley Online Library on [13/05/2025]. See the Terms and Conditions (https://onlinelibrary.wiley.com/terms-and-conditions) on Wiley Online Library for rules of use; OA articles are governed by the applicable Creative Commons License

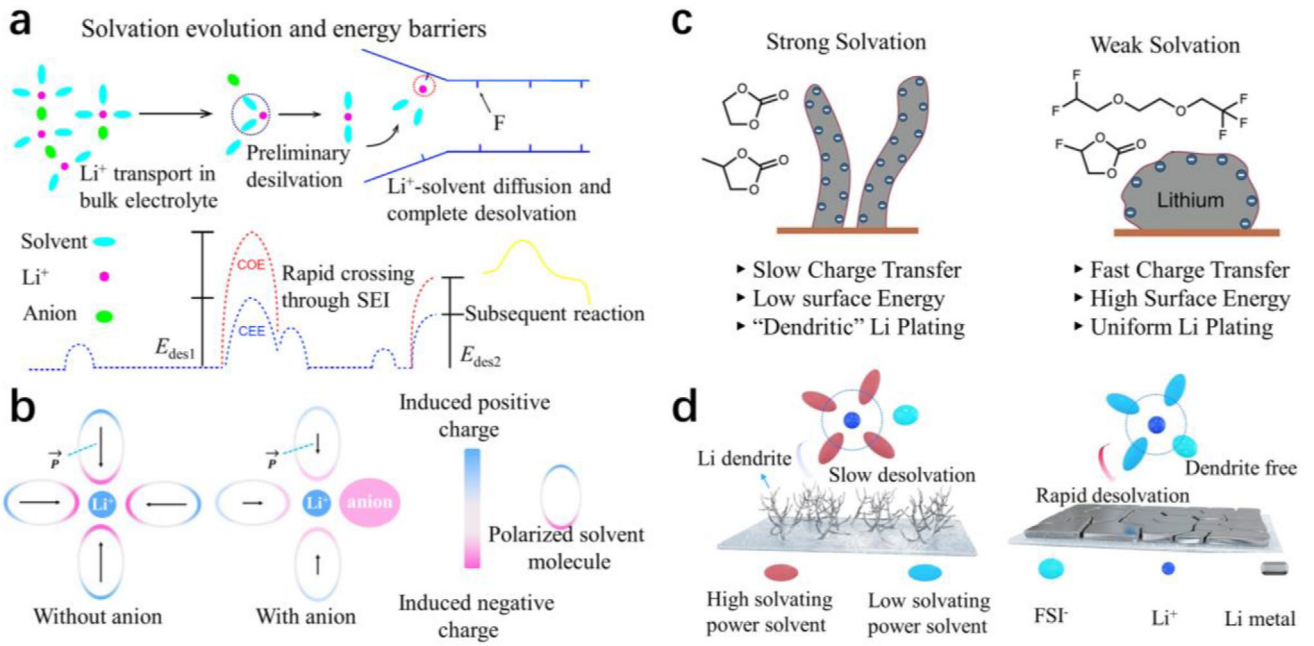

Figure 3. a) Reduction in the difficulty of the desolvation process; Reproduced with permission.[44] Copyright 2023, Springer Nature. b) Reduction in solvent polarization; Reproduced with permission.[45] Copyright 2022, John Wiley & Sons. c) Improvement of lithium plating kinetics; Reproduced with permission.[24] Copyright 2022, American Chemical Society. d) Construction of inorganic-rich electrode/electrolyte interphase; Reproduced with permission.[43] Copyright 2022, John Wiley & Sons.

2.3. Basic Principles of WSE

Generally, there are two effective strategies for designing WSE: minimizing the interaction between metal cations and solvents, and enhancing the interaction between metal cations and anions.[46] The fundamental principle in the design of WSE is to regulate and balance the interaction between metal cations and solvent, as well as between metal cations and anions.[39] This is achieved by using weakly solvating solvents to decrease the binding energy between metal cations and solvents, and low dissociation salts to strengthen the interaction between metal cations and anions (**Figure 4a**).[47]

In the design of WSEs, their components are typically screened based on three parameters: donor number (DN), dielectric constant (ε), and electrostatic potential (ESP). The donor number reflects the attraction of electrolyte components to metal cations and can also assess the ability of the solvent to dissolve salts.[48,49] In WSE, salts and solvents with generally low to medium DN values are chosen. Salts with high DN values are difficult to dissociate, and solvents with high DN values indicates overly strong interaction with metal cations, making them unsuitable for WSE. When selecting anions and solvents with a considerable DN, anions can easily enter the solvation sheath, increasing the reduction stability of the electrolyte, i.e., a high ionic conductivity of 5.42 mS cm^{-1} in $LiNO_3$/TMP (trimethyl phosphate) weakly solvating electrolyte was achieved with NO_3^- anions (DN: 22.2 kcal mol^{-1}) and TMP (DN: 23 kcal mol^{-1}).[45] In terms of dielectric constant, solvents with a medium-low ε are generally selected. Too high dielectric constant values lead to increased viscosity and slower ion migration, while too low dielectric constant values make it difficult to dissolve salts, resulting in a loss of ionic conductivity. The solvent selection for WSE should aim to minimize the desolvation energy while ensuring ionic conductivity.[50] In Figure 4b,c, graphs of DN values, ε values, and the relationship between Li^+-solvent binding energy and ε are presented. The effective screening of solvents with lower DN and medium-low dielectric constants (IV region) significantly reduces the Li^+-solvent affinity without sacrificing dynamic transport.[51] However, DN values and dielectric constants cannot ensure a completely accurate assessment of whether the selected solvent meets the requirements of WSE. ESP can address this deficiency. The absolute value of the lowest negative ESP (|ESPmin|) reflects the solvent's desolvation ability, while the highest positive ESP (ESPmax) represents the polarization of the solvent. When |ESPmin|>ESPmax, it indicates a strongly solvating solvent; when |ESPmin|<ESPmax, it indicates a non-solvating solvent. However, when |ESPmin| is roughly equal to ESPmax and minimized as much as possible, it suggests suitability for use as a WSE solvent, as exemplified in the bottom-left region of Figure 4d,e.[52]

2.4. Salt and Additive Engineering in WSE

WSEs utilize lithium salts with low dissociation energy and high solubility.[3] For example, $LiNO_3$ is a commonly used low-dissociation-energy salt that offers advantages such as low cost, low corrosiveness, and anodic film-forming functionality.[53] Another common low-dissociation-energy salt, i.e., lithium triflate (LiOTF), lithium difluoro(oxalate)borate (LiDFOB), lithium bis(fluorosulfonyl)imide (LiFSI), and lithium difluorophosphate (LiDFP). In addition, there are some newly synthesized

© 2025 The Author(s). Advanced Energy Materials published by Wiley-VCH GmbH

16146840, 0, Downloaded from https://advanced.onlinelibrary.wiley.com/doi/10.1002/aenm.202501272 by Karlsruher Institut Für Technologie, Wiley Online Library on [13/05/2025]. See the Terms and Conditions (https://onlinelibrary.wiley.com/terms-and-conditions) on Wiley Online Library for rules of use; OA articles are governed by the applicable Creative Commons License

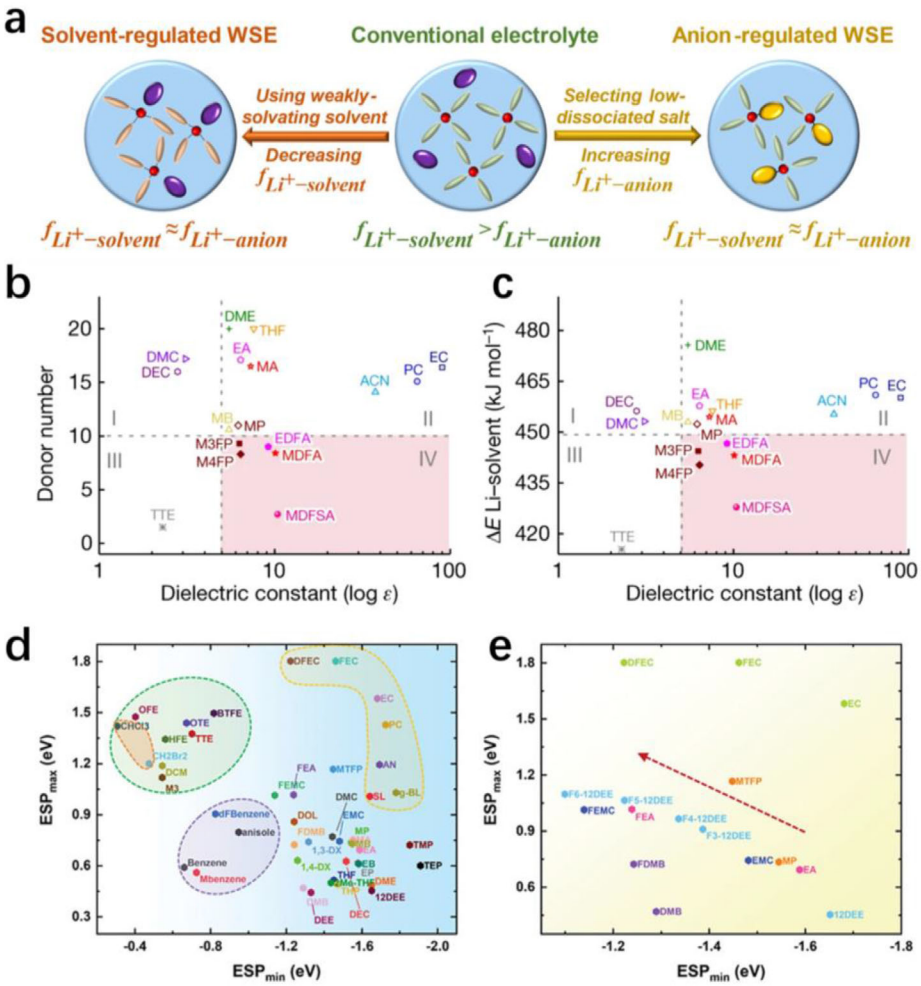

Figure 4. a) Comparison of the solvation structures of different electrolytes; Reproduced with permission.[47] Copyright 2023, John Wiley & Sons. The relationship between the dielectric constants and b) DN values and c) Li^+-solvent binding energy of different solvents; Reproduced with permission.[51] Copyright 2023, Springer Nature Limited. d) Density functional theory-calculated ESP of various solvents under vacuum conditions. e) ESP of fluorinated solvents; Reproduced with permission.[52] Copyright 2023, John Wiley & Sons.

lithium salts, such as a novel cyanide-functionalized LiDFOB analog, lithium difluoro(1,2-dihydroxyethane-1,1,2,2-tetracarbonitrile)borate (LiDFTCB) (**Figure 5a**). In the LiDFTCB-based electrolyte, excessive decomposition of the salt is effectively suppressed, and a relatively thin SEI/CEI layer is formed on the surface of Graphite ||$LiCoO_2$. When using LiDFTCB-PC in a Graphite ||$LiCoO_2$ full cell for 600 cycles, it showed a high-capacity retention of 80.2% and a high average Coulombic efficiency (CE) of 99.9% (Figure 5b).[54]

Regarding research on WSE additives, it has been reported that by adding insoluble nano-particles of Li_3N to the reference electrolyte (RE, $LiPF_6$-EC/DEC-FEC) ($LiPF_6$: lithium hexafluorophosphate; EC: ethylene carbonate; DEC: diethyl carbonate; FEC: fluoroethylene carbonate), a suspension electrolyte (Li_3N SE) can be produced. The nanoparticle of Li_3N in the suspension weakens the Li^+-solvent interactions and reduces the coordination number of the solvent, promoting the desolvation of Li^+. At the same time, it reduces the production of organic compounds in the SEI (Figure 5c). This functional additive also optimizes lithium deposition with relatively dense and bulk particle morphology (Figure 5d).[55]

2.5. Selection and Variety of WSS

In the design of WSE, compared to limited research reports on salt engineering and additive engineering, research on solvent engineering is more extensive. So far, research reports on WSS can be categorized into two main types: existing commercial solvents and new synthetic solvents. Among existing solvents, research on ether-based solvents is the most comprehensive, followed by fluorine-containing solvents, as well as silicon-based solvents.

2.5.1. Ether-Based Weakly Solvating Solvents

Compared to conventional electrolytes, ether-based solvents have the advantages of low freezing point and viscosity, hence, they

© 2025 The Author(s). Advanced Energy Materials published by Wiley-VCH GmbH

16146840, 0, Downloaded from https://advanced.onlinelibrary.wiley.com/doi/10.1002/aenm.202501272 by Karlsruher Institut Für Technologie, Wiley Online Library on [13/05/2025]. See the Terms and Conditions (https://onlinelibrary.wiley.com/terms-and-conditions) on Wiley Online Library for rules of use; OA articles are governed by the applicable Creative Commons License

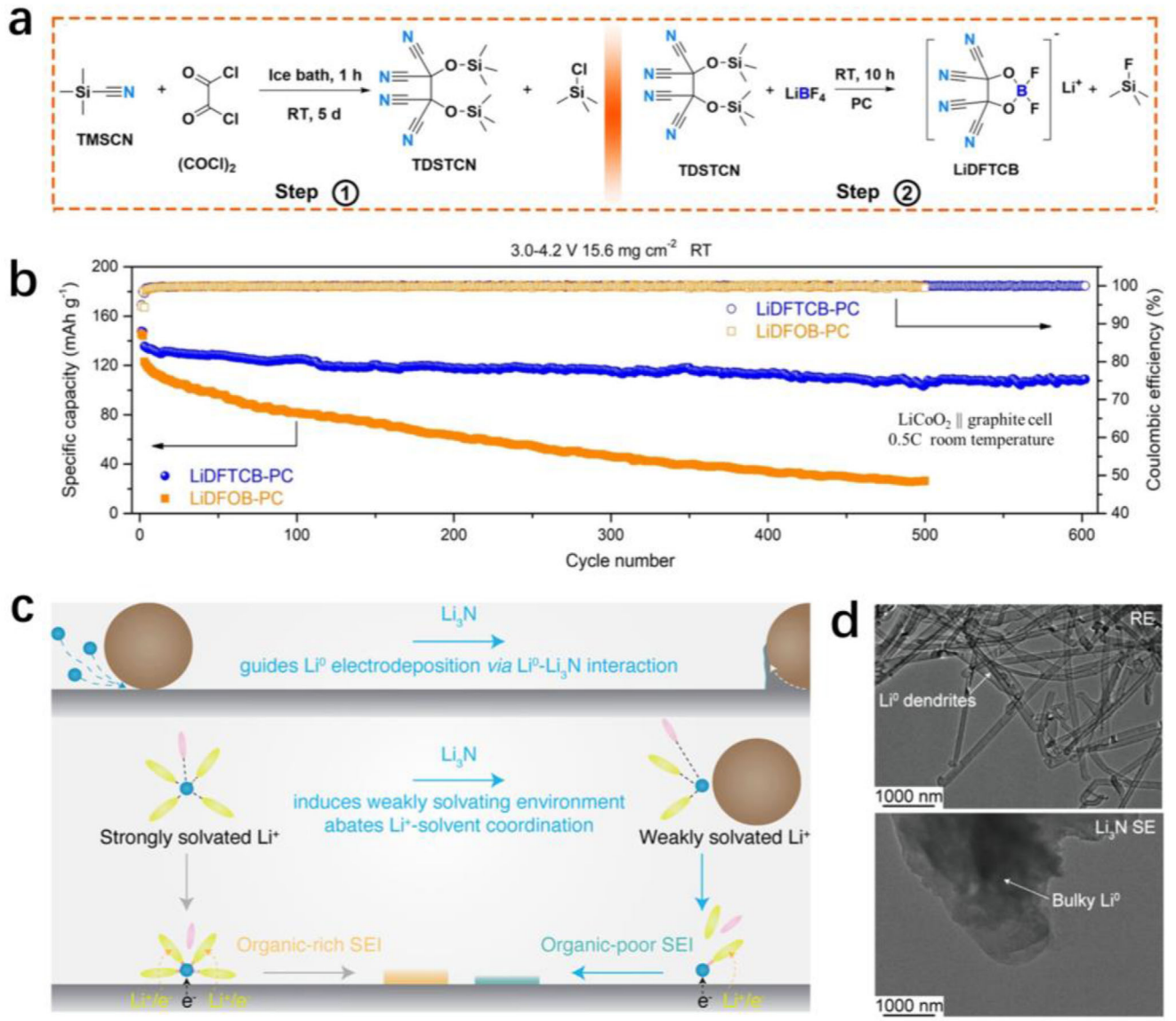

Figure 5. a) Two-step synthesis procedure of LiDFTCB-PC. b) Cycling performance of the different electrolytes; Reproduced with permission.[54] Copyright 2023, John Wiley & Sons. c) Functional schematic diagram of Li_3N. d) Low magnification cryo-TEM image of Li^0 electrodeposits on Cu TEM grid with RE and Li_3N SE; Reproduced with permission.[55] Copyright 2023, American Chemical Society.

are utilized more in low-temperature environments. However, traditional ether solvents fail to meet the requirements for rapid desolvation during the charge–discharge process. The main reason is the strong interaction between traditional ether solvents and Li^+, which requires rational design on ether molecules. Summarizing current research on designing ether-based WSEs, four key aspects are influential: decreasing the number of ether oxygen atoms, increasing the number of non-solvating alkyl groups, shortening the main alkyl chain, and introducing steric hindrance groups into ether molecules.[37,56]

A partially weakly solvating electrolyte (PWSE) composed of LiFSI-DME/TFEE (TFEE: 1,2-bis(1,1,2,2-tetraefluoroethoxy)ethane) has been designed to enhance the desolvation at low temperature and improve stability at high-temperature by weakening the chelation of Li^+ and DME.[57] This modification allows the battery to operate in a wide temperature range (−20–60 °C) and high voltage (4.4 V vs Li/Li^+). The chelating agent TFEE serves as a steric hindrance controller, facilitating fast Li^+ diffusion to the lithium metal anode (LMA) during lithium plating while prohibiting the decomposition of DME solvent. Additionally, lithium fluoromalonato(difluoro)borate (LiFMDFB) and $AgNO_3$ are used as additives to strengthen the electrode/electrolyte interphase and enhance oxidation durability, as illustrated in **Figure 6**a. Recently, a "4S" WSE has been constructed by employing four different ethers: DME, 2-MeTHF (2-methyltetrahydrofuran), THP (tetrahydropyrane), and 1,4-DX.[58] The cyclic and symmetric structure of THP, decreases the electron density of the

© 2025 The Author(s). Advanced Energy Materials published by Wiley-VCH GmbH

16146840, 0, Downloaded from https://advanced.onlinelibrary.wiley.com/doi/10.1002/aenm.202501272 by Karlsruher Institut Für Technologie, Wiley Online Library on [13/05/2025]. See the Terms and Conditions (https://onlinelibrary.wiley.com/terms-and-conditions) on Wiley Online Library for rules of use; OA articles are governed by the applicable Creative Commons License

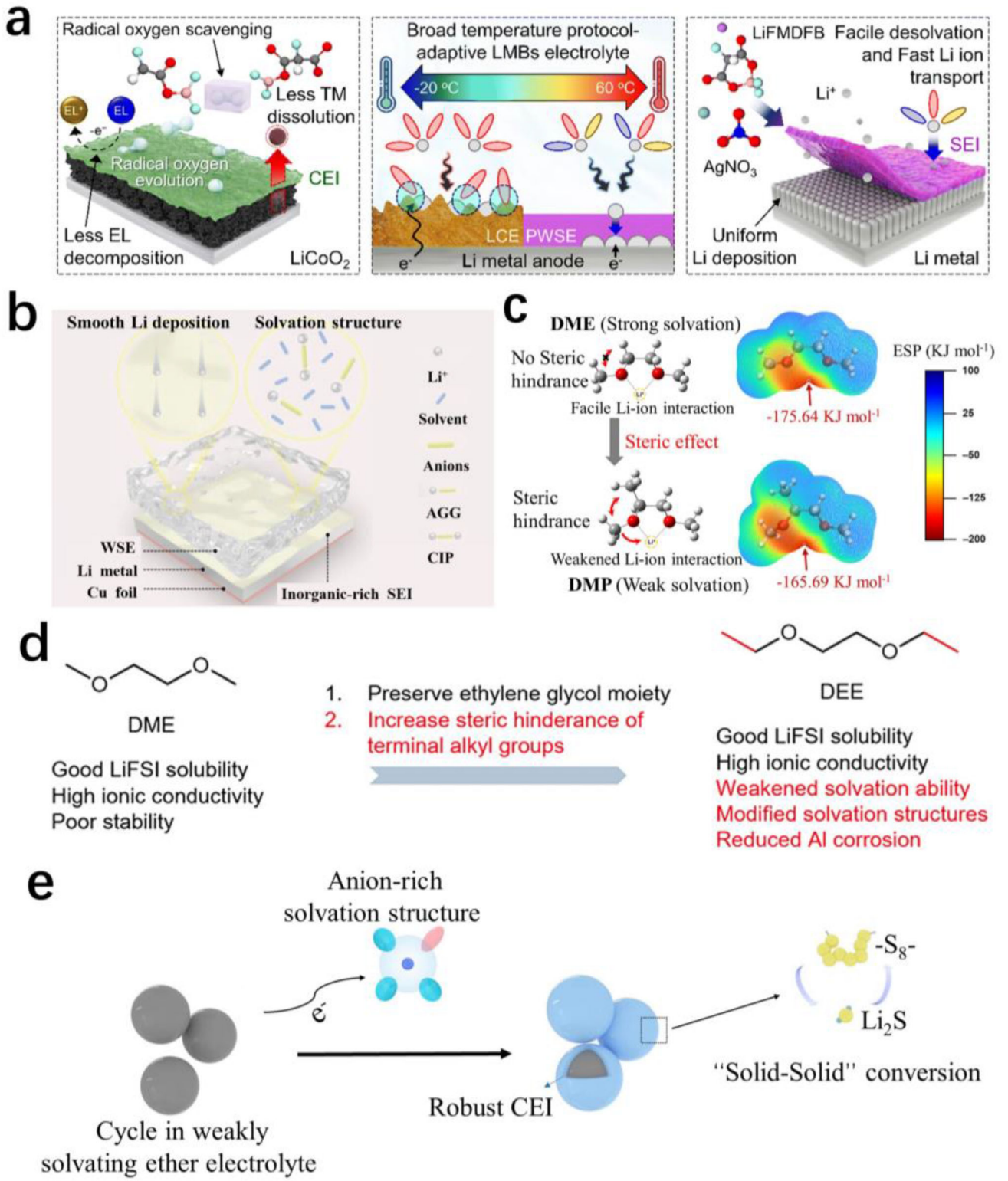

Figure 6. a) Proposed mechanisms of the additive-supplemented PWSE; Reproduced with permission.[57] Copyright 2023, Royal Society of Chemistry. b) Schematic of the weakly solvating electrolyte; Reproduced with permission.[58] Copyright 2023, John Wiley & Sons. c) Schematic illustration of steric hindrance and ESPs of DME and DMP; Reproduced with permission.[56] Copyright 2023, American Chemical Society. d) Molecular structure design of DEE; Reproduced with permission.[37] Copyright 2021, American Chemical Society. e) Conversion mechanism of SPAN in weakly solvating ether electrolyte; Reproduced with permission.[59] Copyright 2023, John Wiley & Sons.

© 2025 The Author(s). Advanced Energy Materials published by Wiley-VCH GmbH

16146840, 0, Downloaded from https://advanced.onlinelibrary.wiley.com/doi/10.1002/aenm.202501272 by Karlsruher Institut Für Technologie, Wiley Online Library on [13/05/2025]. See the Terms and Conditions (https://onlinelibrary.wiley.com/terms-and-conditions) on Wiley Online Library for rules of use; OA articles are governed by the applicable Creative Commons License

oxygen atom in the C—O—C group, thus weakening its solvating ability. This effect promotes the accumulation of anions within solvation shells, forming a LiF-rich SEI layer on the lithium anode surface, which contributes to uniform lithium deposition (Figure 6b).

Among numerous ether-based weakly solvating solvents, linear ethers possess unique advantages. Their diverse molecular structures offer more possibilities for the design of WSE, and the stability of linear ethers surpasses that of cyclic ethers. DME is a typical linear solvent; the utilization of the steric hindrance effect in the modification of DME led to a novel low dielectric constant solvent, 1,2-dimethoxypropane (DMP) (Figure 6c).[56] Compared to DME, the solvating ability of lithium ions is reduced, achieving highly reversible plating/stripping behavior on lithium metal and significantly enhancing the overall cycling stability. The linear ether solvent DMM (dimethoxymethane) also exhibits a weakly solvating ability, which markedly improves lithium deposition behavior at low temperatures, demonstrating higher reversibility of lithium plating/stripping. Even at −40 °C, the Li||Cu cell exhibits a high CE of 97.97%.[43] By replacing the methoxy group in DME with a larger ethoxy group, the DEE solvent, characterized by steric hindrance, was developed (Figure 6d).[37] The full cell, coupled with a high areal capacity of 4.8 mAh cm^{-2} NMC811 and 50 μm lithium maintained 80% capacity retention for 182 cycles, while the 4 M LiFSI/DME configuration retained only 94 cycles, showcasing a viable route for the molecular design of practical high-voltage LMBs with non-fluorinated ether-based electrolyte. In lithium-sulfur batteries, carbonate electrolytes exhibit excellent stability with sulfurized polyacrylonitrile (SPAN), but suffer from serious compatibility issues with the lithium metal anode, greatly affecting the overall electrochemical performance of the battery. A low-concentration ether-based electrolyte (LiFSI-BME; BME: butyl methyl ether) has been developed that can meet the requirements of both the SPAN cathode and lithium metal anode. This electrolyte enables the formation of a robust CEI on the surface of SPAN to block the dissolution of polysulfides, allowing SPAN to undergo reversible "solid–solid" conversion in ether-based electrolytes (Figure 6e), supporting the stable operation of Li||SPAN pouch cells for over a month under the conditions of electrolyte deficiency and 5% excess lithium.[59]

2.5.2. Fluorinated Weakly Solvating Solvents

The electrolytes with fluorinated solvents have been investigated owing to their significant influence on the electrochemical properties of batteries.[60] The strong electron-withdrawing nature of fluorine in fluorinated solvents has an impact on their solvating ability, the Li^+ solvating ability of fluorinated solvents is lower than that of non-fluorinated solvents.[61] The diminished solvating ability of fluorinated solvents is mainly attributed to the fluorine atoms reducing the local electron density around Li^+ coordination sites in the solvent. Additionally, fluorinated solvents exhibit an enhancement in oxidative stability and flammability. Importantly, the decomposition of fluorinated solvents and anions tends to form an inorganic-rich electrode/electrolyte interphase layer.[25,62,63] Furthermore, the weakly solvating property facilitates the forward transfer of Li/Li^+ equilibrium potential and increases the surface energy of Li, promoting uniform lithium deposition.[24]

Fluorinated ethers are more commonly used as anti-solvents or diluents in electrolytes due to their low solubility and solvating ability. Fluorinated carboxylic esters with high boiling points and low melting points have attracted attention in the study of WSE. They exhibit good compatibility with graphite/Li anodes and high-voltage cathodes. Additionally, solvents based on fluorinated sulfonamides, such as N, N-dimethyl trifluoromethanesulfonamide,[64] fluorinated amides, and 2,2,2-trifluoro-N, N-dimethylacetamide,[65] are also categorized as weakly solvating solvents. They possess lower solvating ability and readily form SEI/CEI layers enriched with inorganic compounds like LiF on the electrolyte/electrode interphase. Besides, typical representatives of fluorinated linear carbonates WSEs include bis(2,2,2-trifluoroethyl) carbonate (BTFC),[66] and 2,2,2-trifluoroethyl methyl carbonate (FEMC).[67]

However, using a single fluorinated solvent poses issues such as high viscosity and low ionic conductivity. Thus, considering the overall performance of the battery, fluorinated solvents are not used alone but instead mixed with other fluorinated or conventional solvents in most reported WSEs. For example, a LiFSI-EDFA/FEC WSE prepared using ethyl difluoroacetate (EDFA, weak solvation energy: 15.0 kcal mol^{-1}) with FEC achieves excellent performance in LIBs under the harsh conditions of high voltage, high rate, and wide temperature range (**Figure 7a,b**).[68] Cao et al. developed a mixed weakly solvating solvent FEC/BTFC/ETFA (ETFA: ethyl trifluoroacetate) (volume ratio of 2:2:6). In this work, the fluorinated form of FEC/BTFC reduces the solvating ability of the electrolyte and provides a source of F at the electrode/electrolyte interphase. Meanwhile, ETFA exhibits low viscosity, low freezing point, and an ultra-low solvating ability due to the substitution of three H atoms by F, further weakening the Li^+-solvent interactions, enhancing anion involvement in the solvation sheath, and forming an inorganic-rich SEI. (Figure 7c).[66] The influence of the substitution position and degree of fluorine atoms in EA (ethyl acetate) solvents on electrochemical performance has been studied (Figure 7d). After comparing the physical, chemical, and electrochemical performance, trifluoroethyl acetate (EA-f) exhibited excellent low-temperature performance and high oxidative stability. The WSE of 1 M $LiPF_6$ EA-f/FEC greatly improved the cycle life and rate performance of Graphite||NMC622 cells.[69]

2.5.3. Silicon-Based Weakly Solvating Solvents

In recent years, silicon-based electrolytes have shown potential applications in WSEs. Dimethyl dimethoxy silane (DMSi: dimethyl dimethoxy silane, dielectric constant of 3.66) was demonstrated to possess a solvation structure rich in anions.[70] Extending the methyl groups of DMSi to ethyl groups (corresponding to dimethoxy(dimethyl)silane), the reversibility of Li is increased from 97.0% to 99.6%. Furthermore, by replacing the methyl group in DMSi with a trifluoropropyl group, dimethoxy(methyl)(3,3,3-trifluoropropyl)silane solvent can be obtained, effectively improving the cycle stability of Li||$LiCoO_2$ at high voltage (4.6 V).[71] This also provides a reference for the

© 2025 The Author(s). Advanced Energy Materials published by Wiley-VCH GmbH

16146840, 0, Downloaded from https://advanced.onlinelibrary.wiley.com/doi/10.1002/aenm.202501272 by Karlsruher Institut Für Technologie, Wiley Online Library on [13/05/2025]. See the Terms and Conditions (https://onlinelibrary.wiley.com/terms-and-conditions) on Wiley Online Library for rules of use; OA articles are governed by the applicable Creative Commons License

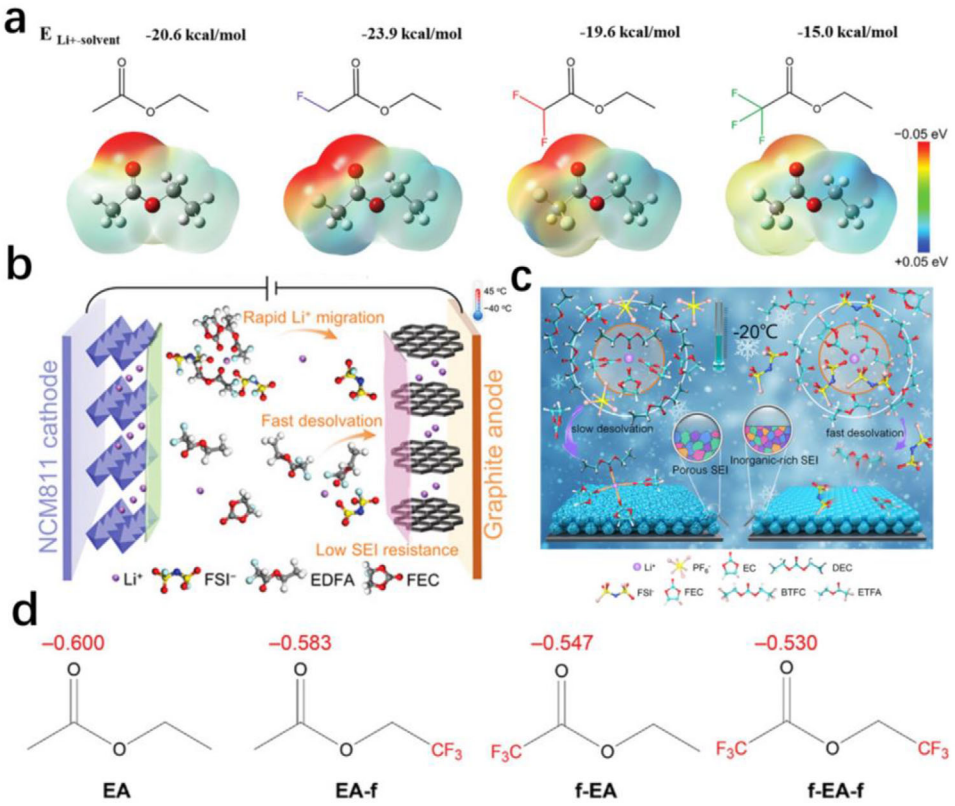

Figure 7. a) ESP maps of different solvents and binding energy of different Li^+-solvent complexes. b) Schematic illustration of the Gr||NCM811 cell with EDFA/FEC electrolyte; Reproduced with permission.[68] Copyright 2023, John Wiley & Sons. c) Schematic illustration of the solvation structures of different electrolytes of the (left) 1 M $LiPF_6$-EC/DEC and (right) 1 M LiFSI-FBE; Reproduced with permission.[66] Copyright 2022, American Chemical Society. d) Atomic charge analysis of carbonyl groups of different solvents; Reproduced with permission.[69] Copyright 2022, John Wiley & Sons.

development of other weakly solvating solvents such as ethers and fluorinated solvents.

2.6. Physical Properties of WSE

WSEs exhibit unique advantages in terms of physical properties, but also face certain limitations. A comprehensive understanding of the strengths and weaknesses of WSE is crucial for the rational design of superior electrolytes.

The flammability of electrolytes is determined by various factors, including electrolyte composition, concentration, purity, and physical state. The composition of the electrolyte is a major influential factor; ether-based electrolytes generally possess high flammability, while those containing fluorine, phosphorus, and silicon compounds are usually less flammable. Introducing fluorine-containing compounds such as ethoxy(pentafluoro)cyclotriphosphazene (PFPN) through the "bulky coordination" is a feasible strategy. The self-extinguishing time (SET) from the electrolyte ignition test for the experimental group and the control group is 0 s g^{-1} and 144 s g^{-1}, respectively (**Figure** 8a), demonstrating that the fluorine-containing WSE dramatically reduces flammability and enhances the safety of LMBs.[72]

Viscosity is a critical property of liquid electrolytes, significantly affecting battery performance. It influences the wettability of the electrolyte on separators and electrodes, as well as its connection to ion diffusion rates, conductivity, and transference numbers.[77] WSEs possess lower viscosity, which is mainly attributed to the relatively weak chemical bonds formed within the solvent, which are prone to breakage, resulting in weaker interactions between solvent molecules or ions, thereby decreasing viscosity and improving the ionic conductivity to a certain extent. Isobutyronitrile (iBN), due to its low viscosity, high dielectric constant, and high ionic conductivity at low temperatures, is used as a cosolvent in electrolytes. Its effective weak solvating ability promotes the desolvation of lithium ions and enhances charge transfer kinetics.[73] Figure 8b shows the variation of electrolyte viscosity with temperature; even at −40 °C, the viscosity of iBN-75 (iBN content of 75%) is only 4.672 mPa s. Accordingly, the ionic conductivity is significantly enhanced, achieving a conductivity of 1.152 mS cm^{-1} at −70 °C (Figure 8c).[73] At −70 °C, the electrolyte supports the Graphite||$LiCoO_2$ pouch cell to deliver 68.7% of its room-temperature capacity.

However, it should be noted that the ionic conductivity of WSE is not sufficient in the entire electrolyte system and requires further improvement. An amphiphilic molecule TFMP (1,1,2,2-tetrafluoro-3-methoxypropane) with weak solvating ability, was designed by Shi et al., which can induce self-assembly to form a unique "core-shell" solvation structure. The electrolyte containing TFMP shows an increased ionic conductivity from 0.8 to 1.8 mS cm^{-1} compared to the reference

© 2025 The Author(s). Advanced Energy Materials published by Wiley-VCH GmbH

16146840, 0, Downloaded from https://advanced.onlinelibrary.wiley.com/doi/10.1002/aenm.202501272 by Karlsruher Institut Für Technologie, Wiley Online Library on [13/05/2025]. See the Terms and Conditions (https://onlinelibrary.wiley.com/terms-and-conditions) on Wiley Online Library for rules of use; OA articles are governed by the applicable Creative Commons License

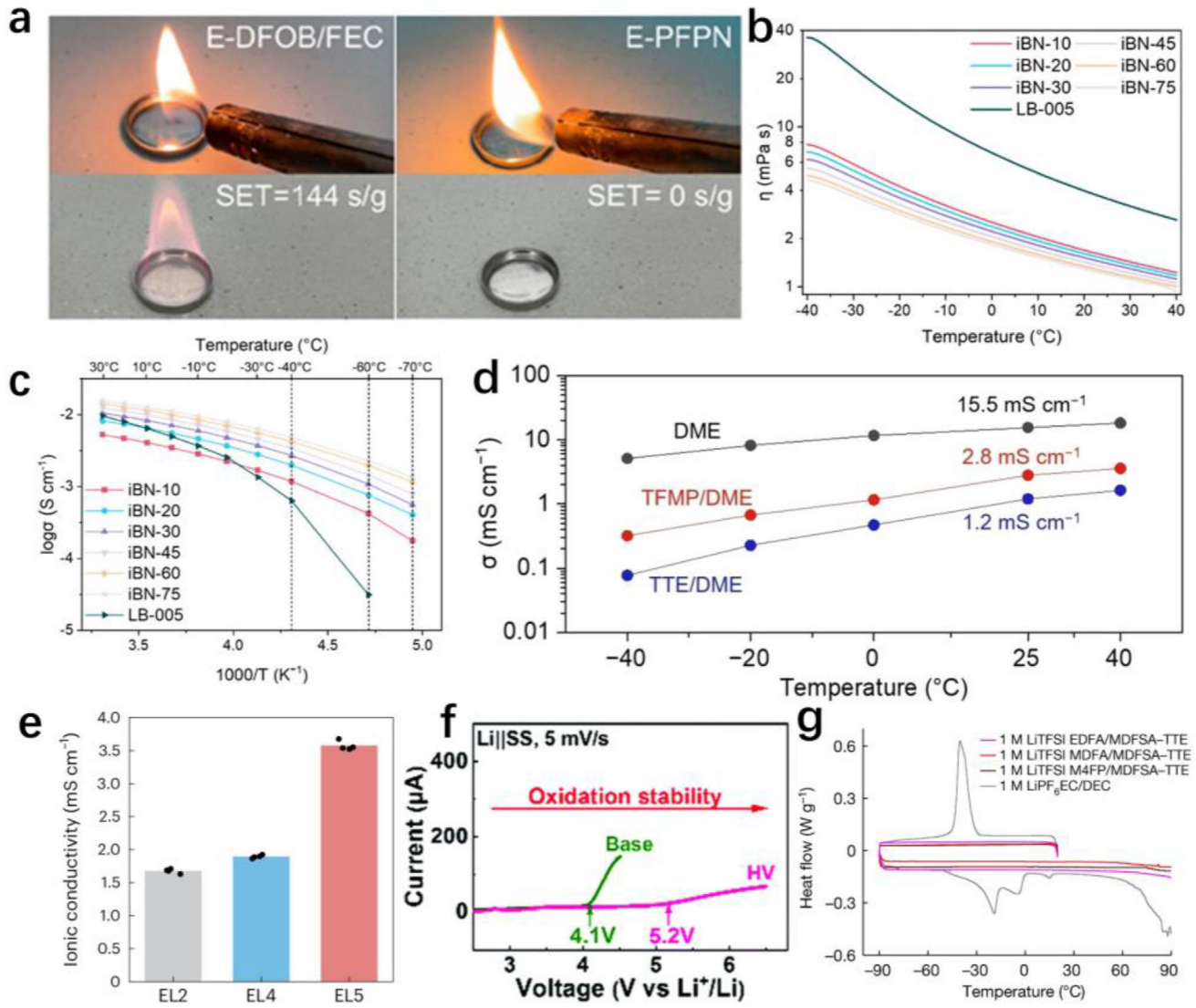

Figure 8. a) Flammability test of (left) E-DFOB/FEC and (right) E-PFPN; Reproduced with permission.[72] Copyright 2023, American Chemical Society. b) Viscosity and c) ionic conductivity with different electrolytes; Reproduced with permission.[73] Copyright 2023, John Wiley & Sons. d) Ionic conductivity of the electrolytes at different temperatures; Reproduced with permission.[74] Copyright 2023, John Wiley & Sons. e) Ionic conductivity in different numbers of solvents; Reproduced with permission.[75] Copyright 2023, Springer Nature Limited. f) Oxidation stability of different electrolytes; Reproduced with permission.[76] Copyright 2022, Royal Society of Chemistry. g) DSC cooling and heating curves of different electrolytes; Reproduced with permission.[51] Copyright 2023, Springer Nature Limited.

electrolyte containing TTE/DME (TTE: 1,1,2,2,2-tetrafluoroethyl-2,2,3,3-tetrafluoropropyl ether). However, its conductivity is inadequate compared to the pure DME-based electrolyte with a conductivity of 15.5 mS cm^{-1} (Figure 8d).[74] In contrast, based on the Raman shift and dielectric constant of the solvents, a novel electrolyte with a multi-level solvation structure has been proposed using the hybrid strongly-weakly-solvating solvent rule. The designed hierarchical solvation structure (DMSi:FEC:TTE = 7:3:5, v/v), named SiFT solvent, demonstrated improved ionic conductivity compared to previously reported WSEs, with a value of 4.28 mS cm^{-1}.[78] Similar work reported by Kim et al. proposed a design strategy to heighten the performance of LMBs by increasing the diversity of electrolyte molecules, essentially deemed as high-entropy electrolytes.[75] Overall, WSEs possess high stability but low ionic conductivity, while the inverse relationship is observed in solvated electrolytes. Nevertheless, compared to traditional WSE (EL2, 1 M LiFSI in DME-TTE), the ionic conductivity of high-entropy electrolyte with smaller cluster size doubled (EL5, 1 M LiFSI-DME-DEE-DEGDME-TTE-BTFE) (Figure 8e).

The electrochemical stability window (ESW) of WSE is of paramount importance for developing high-voltage batteries. The selection of lithium salt, electrolyte, and electrode material typically effect the ESW. For instance, selecting the solvents with a wide HOMO-LUMO energy level gap (HOMO: highest occupied molecular orbital; LUMO: lowest unoccupied molecular orbital) can broaden their potential ESW.[79] A high-voltage

© 2025 The Author(s). Advanced Energy Materials published by Wiley-VCH GmbH

16146840, 0, Downloaded from https://advanced.onlinelibrary.wiley.com/doi/10.1002/aenm.202501272 by Karlsruher Institut Für Technologie, Wiley Online Library on [13/05/2025]. See the Terms and Conditions (https://onlinelibrary.wiley.com/terms-and-conditions) on Wiley Online Library for rules of use; OA articles are governed by the applicable Creative Commons License

electrolyte, consisting of 1 M $LiPF_6$ in a mixture of FEC and bis (2,2,2-trifluoroethyl) carbonate (BTC), which not only exhibits outstanding safety but also widens the ESW.[76] Compared to the solvent in base electrolyte, the HOMO level in high-voltage electrolyte is lower and the HOMO-LUMO energy gap is wider, indicating its superior high-voltage stability. This claim is further supported by linear sweep voltammetry (LSV) results, showing that the voltage window of the electrolyte expands from 4.1 V in base electrolyte to 5.2 V (Figure 8f). Furthermore, studies have revealed that the low dissociation of $LiBF_4$ can form a solvating sheath rich in anions, thereby generating anion-derived interphases. Benefiting from this unique solvation structure and interfacial chemistry, this $LiBF_4$-based WSE successfully matched Li||$LiCoO_2$ full cells under practical conditions, enabling stable cycling at a cutoff voltage of 4.6 V and addressing the challenge of poor oxidative stability in ether-based electrolytes.[47] Furthermore, Gao et al. studied TFP-based (tris(2,2,2-trifluoroethyl) phosphate) weakly solvating electrolytes, which directly broaden the voltage window of potassium batteries to 4.9 V.[80]

Thermal stability is another crucial factor closely associated with the safety of electrolytes, apart from flammability and ESW. Generally, the thermal stability of electrolytes can be evaluated using thermal analysis methods such as differential scanning calorimetry (DSC), thermogravimetric analysis (TGA), and differential thermal analysis (DTA). The thermal stability of an electrolyte is related to factors such as its composition, molecular structure, and chemical bond structure. For instance, $LiPF_6$ exhibits poor thermal stability and is prone to decomposition at high temperatures, producing PF_5 and HF. One solution is to add highly active additives to inhibit the decomposition of $LiPF_6$,[81] or to replace $LiPF_6$ with boron-based lithium salts. Xu et al. proposed a strategy for electrolyte design based on a set of WSS, which balances weak Li^+-solvent interactions, salt dissociation, and electrochemical performance. The designed WSE, LiTFSI MDFA/MDFSA-TTE (LiTFSI: bis(trifluoromethane)sulfonimide lithium; MDFA: methyl difluoroacetate; MDFSA: methyl 2,2-difluoro-2 (fluorosulfonyl)acetate), supports battery operation under extreme conditions and shows good thermal stability compared to conventional EC/DEC-based electrolyte.[51] DSC indicates that the WSE does not undergo phase transition in the temperature range of −90 to 90 °C (Figure 8g). The Graphite||NMC811 full cell with this WSE exhibits superior cycling stability and capacity retention at different temperatures.

3. WSE in Lithium Batteries

3.1. Solvent Composition

The salt solubility in the solvent depends on whether the interaction of the salt-solvent complex is higher than the sum of the interactions of the anion-cation and the solvent-solvent complex. Most of the WSS have poor solubility and need to be combined with other co-solvents to dissolve the lithium salt. However, some of the WSS can dissolve lithium salt without adding other solvents. Therefore, WSEs can be divided into single-solvent WSE and co-solvent WSE.

3.1.1. Single Solvent WSE

In terms of electrolyte design, the traditional electrolyte configuration comprises lithium salt, solvent, and additives. The simple single-salt/single-solvent electrolyte systems exhibit slightly inferior battery performance compared to multi-salt/multi-solvent electrolyte systems; therefore, a variety of electrolyte additives were developed to enhance the performance. In contrast, the single-salt/single-solvent designing concept can achieve an excellent cell performance in WSE study.

To promote the interfacial chemistry of anion derivatives, apart from increasing the ratio of anions to solvents, we can also reduce the solvation ability of solvents based on the theory of competitive coordination between solvents and anions, thus enabling more anions to bind with Li^+. For example, 1,4-DX possesses a very weak solvation ability, but can dissolve 2.0 M LiFSI. In this study, 1 M LiFSI was dissolved in 1,4-DX, 1,3-DX, and DME, respectively, and found that the free anion (FA) content was as high as 71.3%, and AGG content was zero in the strongly solvated DME electrolyte. The FA content decreased significantly in the 1,3-DX electrolyte with the weakening of the solvation ability (**Figure 9a-b**). Moreover, there was no FA structure in the 1,4-DX based WSE, and this shows a faster charging ability than the commercial electrolyte in the case of graphite electrodes.[19] The 1,4-DX also facilitates the dissolution of dual lithium salts, with the capability to dissolve 0.3 M LiFSI and 0.2 M LiTFSI. Quantum mechanics and classical molecular dynamics simulations reveal that even at ultra-low salt concentrations, the synergistic interactions between the 1,4-DX and the dual salts lead to a significant portion of the salt anions being present in the HCE-like CIPs, AGGs related complexes, ultimately forming a thin, compact, and LiF-rich SEI/CEI layer. This inhibits the adverse reactions at the electrode/electrolyte interphase.[82]

It is well known that an SEI rich in organic components is not conducive to suppressing continuous side reactions at the electrode/electrolyte interphase. LiF, as an excellent ionic conductor, serves as an effective inhibitor against the irreversible parasitic side reactions at the electrode/electrolyte interphase. It plays a crucial role in restraining the dendritic growth and facilitating high CE.[83–85] In general, ether solvents with a low reduction potential support the preferential decomposition of fluoride salts, which results in the formation of an LiF-enriched SEI. DEE, as a weak solvent with a low dielectric constant ($\varepsilon = 3.9$), exhibits higher reduction capability compared to DME, due to the stronger electron-donating characteristics of the ethyl groups in DEE. Additionally, the larger size of the ethyl group contributes to increased spatial site resistance, thereby inhibiting the undesirable reaction between the electrode and electrolyte.[86] In a single-solvent-based WSE (1 M LiFSI-DEE), it was observed that a significant portion of the FSI^- exists in the form of CIPs and AGGs. Furthermore, characteristic peaks of LiF with higher relative intensities were identified at the anode surface in 1 M LiFSI-DEE (Figure 9c-g). This indicates the free FSI^- also participated in the formation of SEI/CEI layer, reducing the adverse side reactions and lithium dendrites formation.[87] Subsequently, by combining the concepts of HCE and WSE, DEE was used as the solvent with LiFSI salt to prepare a 3.5 M high-concentration electrolyte. The electrolyte, termed concentrated WSE, adjusts the solvation structure compared to that achieved at lower salt concentrations.

© 2025 The Author(s). Advanced Energy Materials published by Wiley-VCH GmbH

16146840, 0, Downloaded from https://advanced.onlinelibrary.wiley.com/doi/10.1002/aenm.202501272 by Karlsruher Institut Für Technologie, Wiley Online Library on [13/05/2025]. See the Terms and Conditions (https://onlinelibrary.wiley.com/terms-and-conditions) on Wiley Online Library for rules of use; OA articles are governed by the applicable Creative Commons License

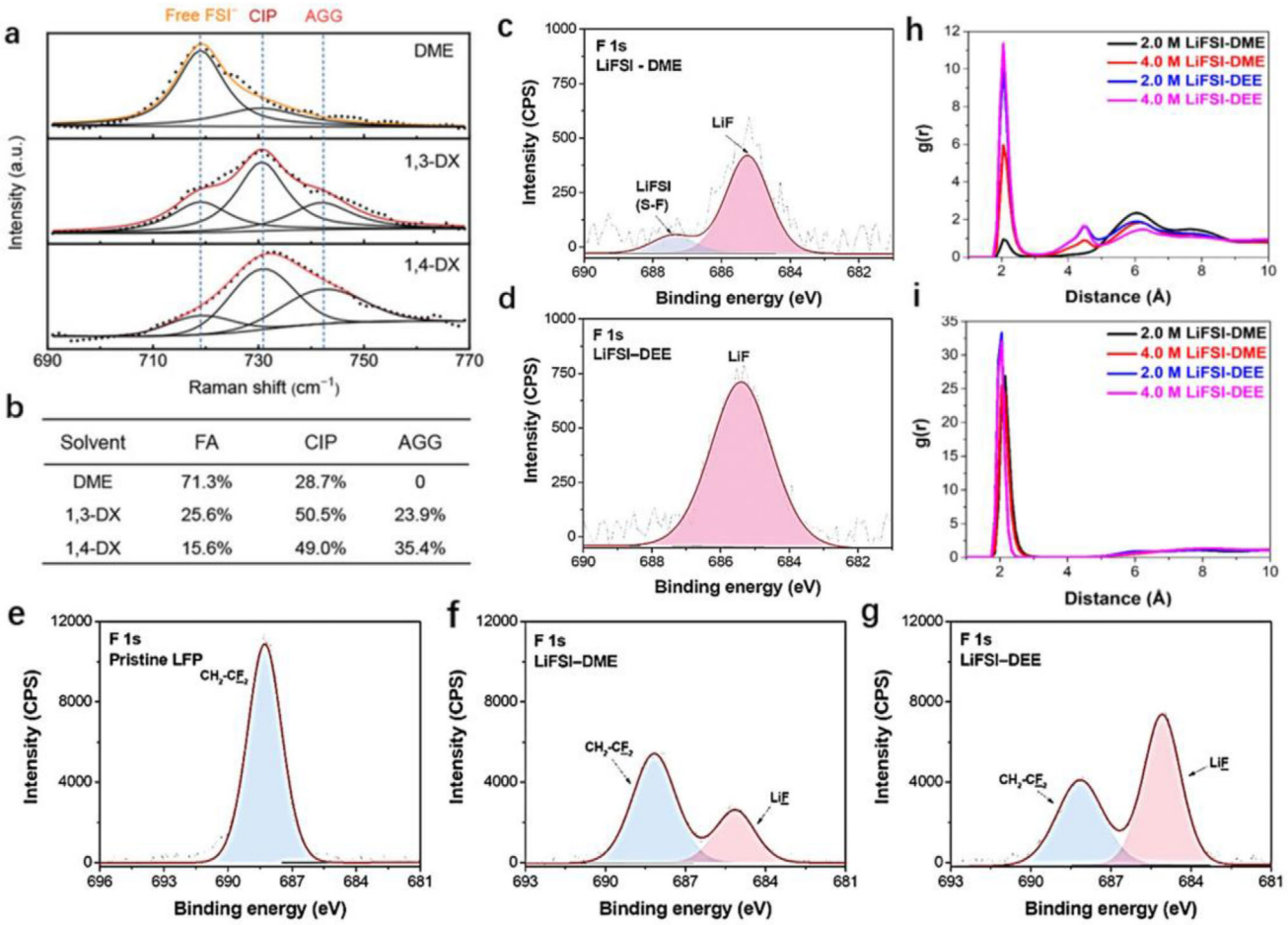

Figure 9. a) Raman spectra and b) solvation structure ratios of different electrolytes. Reproduced with permission.[19] Copyright 2021, John Wiley and Sons. c, d) F 1s XPS spectra of the cycled Li metal anode. e-g) XPS characterization of the CEI components on the LFP electrode after 200 cycles. Reproduced with permission.[87] Copyright 2021, John Wiley and Sons. Radial distribution functions (RDF) between Li^+ and the oxygen atoms of h) FSI^- and i) DME/DEE. Reproduced with permission.[88] Copyright 2021, John Wiley and Sons.

The classical molecular dynamics simulations at both moderate (2.0 M) and high (4.0 M) concentration demonstrate that the number of FSI^- anions in the first solvated shell of Li^+ in LiFSI-DEE is higher than that in LiFSI-DME (Figure 9h,i), which is consistent with the Raman results. Moreover, because of the low reduction potential of the solvent, lithium salt preferentially undergoes decomposition to form a fluorine-rich interfacial layer. Consequently, the Li||NCM811 cell maintains a stable cycling even at 4.4 V.[88] This implies that DEE can be a good candidate for WSE design.

Compared with carbonate-based electrolytes, ether-based electrolytes have higher LUMO energy, leading to superior reduction stability on LMAs.[89,90] However, conventional solvents like DME possess strong solvation ability, which greatly participates in the solvation structure and results in the exacerbation of interfacial solvents decomposition.[37] This can be addressed by employing weakly solvated cyclic ethers to promote more anions into the solvated sheath. THP, a cyclic ether, possesses a spatial structure with more electron-absorbing-groups (C_xH_y) compared to DME. Additionally, THP has a stronger electronegativity and greater spatial resistance, resulting in weak Li^+ coordination ability and generating an anion-rich solvation structure (**Figure 10a**). This effectively promotes the SEI/CEI interphase layer rich in inorganic species, which optimizes the interfacial Li deposition behavior, inhibiting the dissolution of transition metal ions, and generates an undissolved $Al(FSI)_x$ passivation layer on the surface of Al foil to avoid corrosion of the current collector.[91] Peng et al.[92] developed an ether-based electrolyte with $LiPF_6$ as salt. The linear ether solvent ethylene glycol dibutyl ether (EGDE) (**Figure 10b**) with a large steric hindrance effect can reduce the solvation ability with Li^+, thus facilitating the participation of PF_6^- in the solvation sheath. This electrolyte enables the rapid passivation of the micrometer-sized silicon (mSi) anode and the formation of a robust and LiF-rich SEI, hence prolonging the cycle life of the mSi anode.

Ether-based electrolytes tend to form the deposited lithium with large particles and a smoother surface, reducing the contact surface area between the electrolyte and LMA.[94,95] Fluorinated ethers maintain the advantages of ether solvents while enhancing the redox stability, thus facilitating the design of high-voltage electrolytes. Zhao et al. designed a novel solvent by merging a cyclic fluorinated ether with a linear ether segment, known as

© 2025 The Author(s). Advanced Energy Materials published by Wiley-VCH GmbH

16146840, 0, Downloaded from https://advanced.onlinelibrary.wiley.com/doi/10.1002/aenm.202501272 by Karlsruher Institut Für Technologie, Wiley Online Library on [13/05/2025]. See the Terms and Conditions (https://onlinelibrary.wiley.com/terms-and-conditions) on Wiley Online Library for rules of use; OA articles are governed by the applicable Creative Commons License

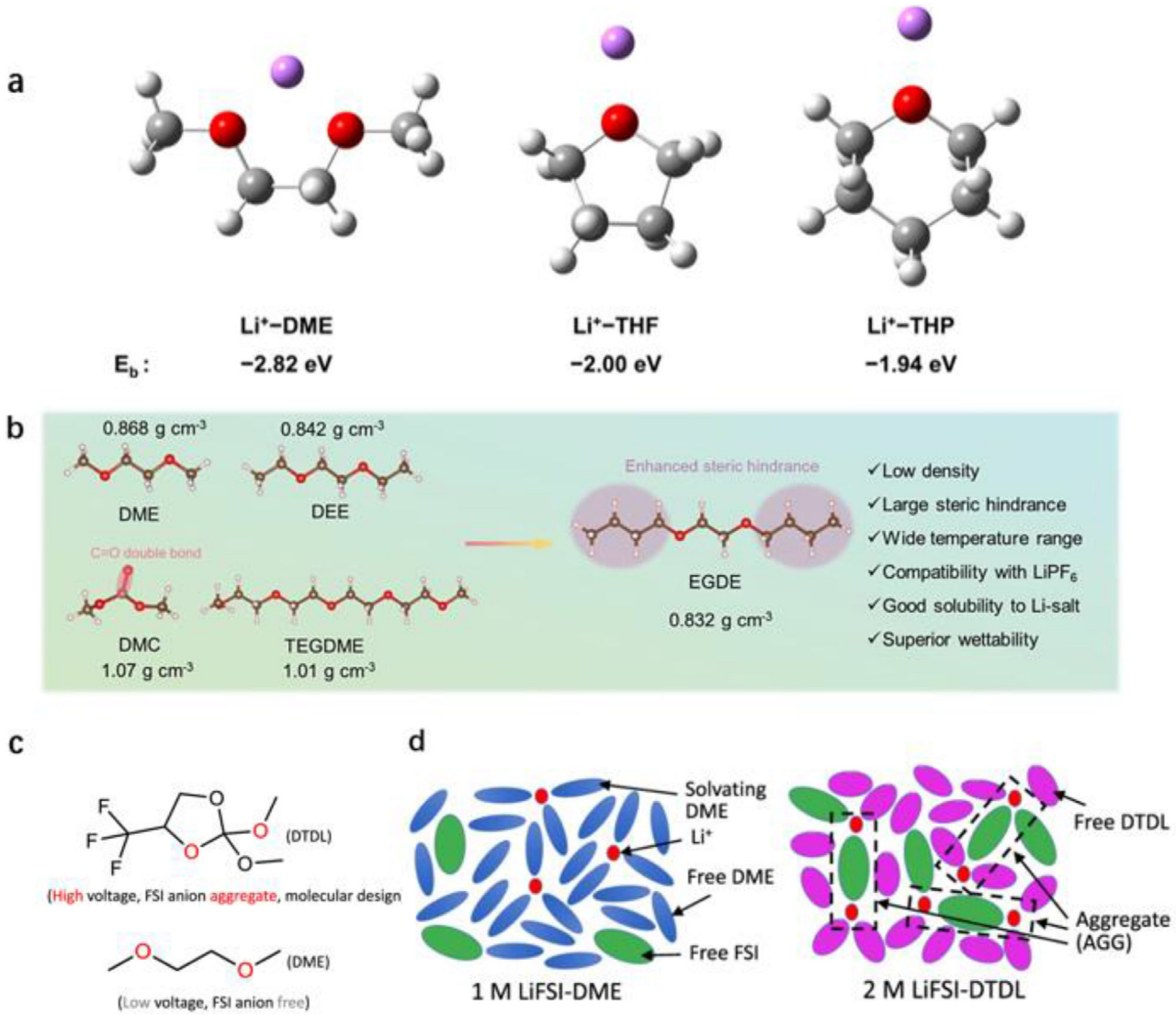

Figure 10. a) Binding energies of Li^+-solvent coordination structures. Reproduced with permission.[91] Copyright 2023, American Chemical Society. b) Schematic illustration of the molecular structure of EGDE. Reproduced with permission.[92] Copyright 2023, American Chemical Society. c) Comparison of molecular structures of DTDL and DME. d) Schematic diagram of the coordination structure of different electrolytes. Reproduced with permission.[93] Copyright 2022, Springer Nature.

2,2-dimethoxy-4-(trifluoromethyl)-1,3-dioxoane (DTDL) (Figure 10c). The oxidative stability of the ether has been improved by introducing an electron-withdrawing functional group, $-CF_3$, and adjusting its spatial arrangement. Additionally, it retains the capability for controlled solvation of lithium ions, achieving an impressive electrochemical window of 5.5 V. The electrolyte of 2 M LiFSI-DTDL results in the formation of numerous CIPs and AGGs (Figure 10d), thereby facilitating a highly stable cycling performance in the Li||NCM811 full cell.[93]

3.1.2. Co-Solvent in WSE

The single-solvent WSE possesses inherently weak solvent properties and has limited capacity to dissolve lithium salts. Therefore, additional solvents are often required to augment the solubility of lithium salts in WSE formulations. Additionally, the combination of multiple solvents can synergistically compensate for the deficiencies of individual solvents. Generally, co-solvents with high dielectric constants are selected, such as the film-forming co-solvent FEC, the presence of an organofluorine group (C-F) generated by the oxidative decomposition of fluorinated solvents also has a positive impact on the electrochemical performance.[96] The use of perfluorinated WSE design with BTFC/FEC/ETFA has resolved the issue of the narrow operating temperature range of silicon-based batteries.[66] Silicon suboxide (SiO_x) is one of the high-potential anode materials that still suffers from volume expansion and unstable electrode/electrolyte interphase formation during long-term cycling. FEC with strong electron-withdrawing of the internal fluorine atom, preferentially decomposes to form

© 2025 The Author(s). Advanced Energy Materials published by Wiley-VCH GmbH

16146840, 0, Downloaded from https://advanced.onlinelibrary.wiley.com/doi/10.1002/aenm.202501272 by Karlsruher Institut Für Technologie, Wiley Online Library on [13/05/2025]. See the Terms and Conditions (https://onlinelibrary.wiley.com/terms-and-conditions) on Wiley Online Library for rules of use; OA articles are governed by the applicable Creative Commons License

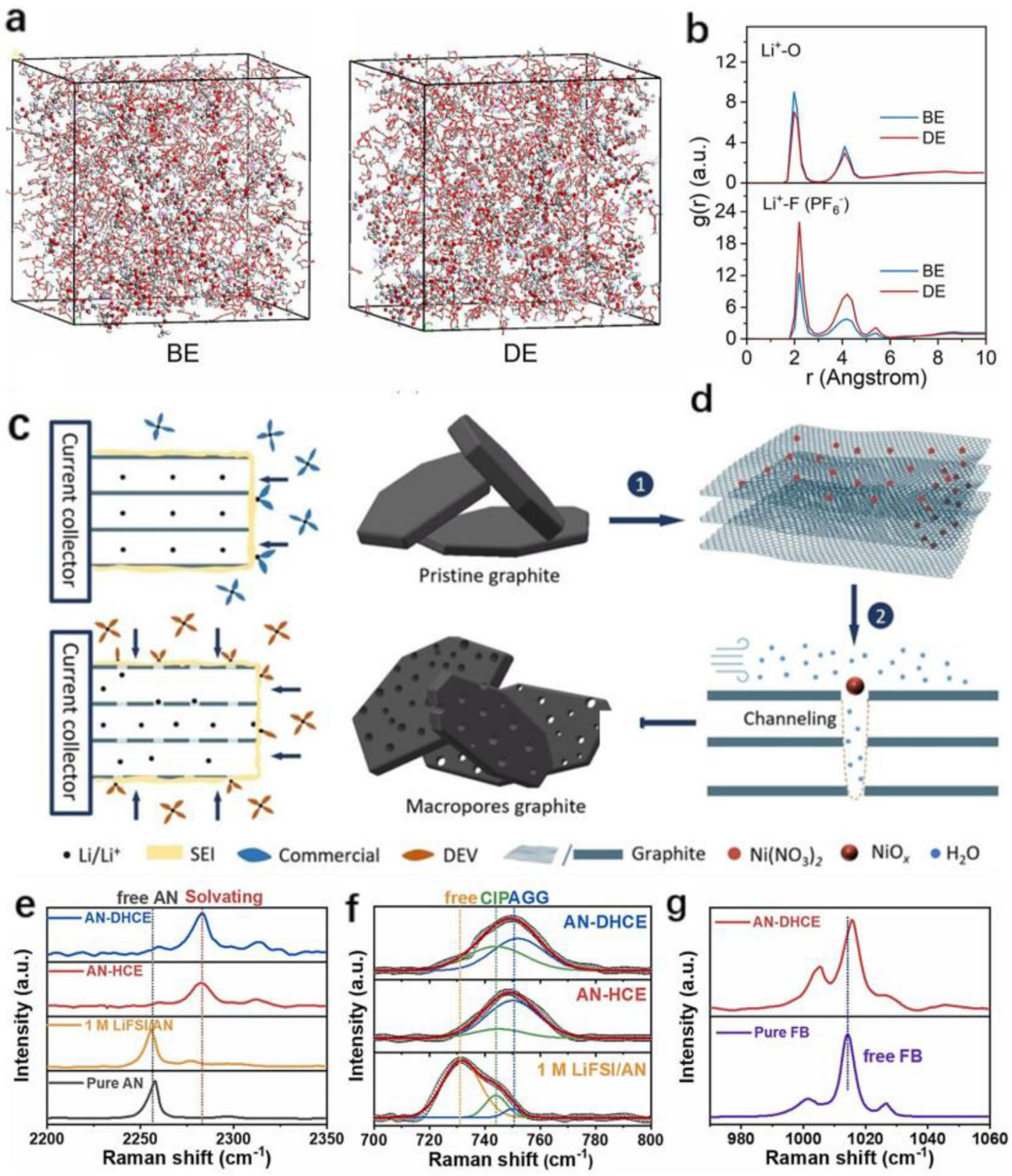

Figure 11. a) Solvation structure of Li^+ affected by FEC co-solvent. b) RDF of Li^+-O and Li^+-F (PF_6^-) in different electrolytes. Reproduced with permission.[99] Copyright 2023, Elsevier. Schematic illustration of Li^+ intercalation process for c) The pristine graphite and macroporous graphite (MPG). d) Preparation process of MPG. Reproduced with permission.[100] Copyright 2023, John Wiley and Sons. e,f) Raman spectra of LiFSI-AN electrolyte. g) Raman spectra of FB and AN-DHCE. Reproduced with permission.[101] Copyright 2022, Elsevier.

© 2025 The Author(s). Advanced Energy Materials published by Wiley-VCH GmbH

16146840, 0, Downloaded from https://advanced.onlinelibrary.wiley.com/doi/10.1002/aenm.202501272 by Karlsruher Institut Für Technologie, Wiley Online Library on [13/05/2025]. See the Terms and Conditions (https://onlinelibrary.wiley.com/terms-and-conditions) on Wiley Online Library for rules of use; OA articles are governed by the applicable Creative Commons License

a stable SEI, thus inhibiting the reductive decomposition of the main solvent of the electrolyte.[97,98] By employing FEC/DMC (dimethyl carbonate) dual-solvent WSE, this revealed that FEC facilitates Li^+ desolvation kinetics through facile access to the primary Li^+ solvation sheath and weaker interaction with Li^+. This phenomenon alters the coordination of Li^+ with PF_6^- anions (Figure 11a,b), increasing the involvement of the anions in SEI formation. Thus, the Li||SiO_x half-cell exhibits outstanding rate performance and high CE.[99]

To mitigate the challenges of poor rate performance and lithium dendrite growth in graphite-based batteries, the cosolvents of DOL, EC, and VC (vinylene carbonate), which are less polar, are employed. Thus, the electrolyte reduces the desolvation energy barrier at the electrode/electrolyte interphase at higher or lower temperatures, facilitating smooth ion migration and rapid diffusion across the interphase (Figure 11c,d). This electrolyte enables fast charging of the graphite with a large pore size (≈100 nm) even at -30 °C.[100] Fluorobenzene (FB) as a co-solvent resolves the challenge of dissolving lithium salts in acetonitrile (AN). With its high dielectric constant, FB guarantees the dissolution of lithium salt. Additionally, the lower binding energy of Li^+-AN enables Li^+ to easily detach from all the surrounding solvent molecules, achieving a balance between solvation and desolvation of lithium ions. Meanwhile, the addition of FB separates the large AGG structure into small ion pairs (Figure 11e–g), which is more favorable for enhancing the diffusion ability of Li^+ in the electrolyte and improving the Li^+ desolvation kinetics. Finally, the Graphite||NCM811 pouch cell achieved 80% capacity retention after 500 cycles.[101] Similarly, in lithium-sulfur batteries, the use of the weak solvent di-isopropyl ether (DIPE) paired with THF aids in dissolving the LiFSI, LiTFSI dual salt system. On account of the weak solvation ability of DIPE, the generated electrolyte exhibits a co-ionization effect that effectively inhibits the dissolution of lithium polysulfides and the self-discharge phenomenon, as well as greatly enhances the cycle life of lithium-sulfur batteries at low temperature.[102]

It is evident that in the realm of single-solvent WSE, there is a tendency to choose ether-based solvents with a lower dielectric constant as the base solvent. This choice enables the electrolyte to exhibit good ionic conductivity while maintaining a certain degree of solubility. Among these solvents, fluorinated ether-based solvents have emerged as a prominent focus of research. Furthermore, researchers tend to develop multifunctional WSS to circumvent the limitations associated with single-solvent. In multi-solvent WSE, fluorinated solvents are favorable for electrode stabilization due to the beneficial LiF component. However, fluorinated solvents typically exhibit low solubility. Therefore, they are ideally paired with ester and ether solvents with slightly stronger polarity to prepare WSE.

3.2. Interactions Between Ions and Solvents

In WSEs, solvent molecules, along with anions and cations, collaboratively construct the microstructure and dynamic behavior of the electrolyte. The interaction between these components exhibits a unique dynamic equilibrium, which is vital for the overall performance of the electrolyte and its interaction with electrodes. Serving as a "bridge," solvent molecules connect ions with electrode surfaces, enabling the stable operation of the entire electrochemical system. Meanwhile, this interaction also provides possibilities for optimizing the performance of electrolytes. For instance, by adjusting the types and proportions of solvents, we can regulate the conductivity, stability, electrochemical window, and other properties of the electrolyte.

3.2.1. Solvents and Cations

In the electrolyte of lithium batteries, solvent molecules typically interact with lithium ions to form Li-solvent complexes. This interaction affects crucial parameters such as the ionic conductivity, ion mobility rate, and lithium ion solubility. In traditional electrolytes, the migration of Li^+ is more difficult due to the strong Li^+-solvent interactions, which maintain Li^+ in a stable solvated state. Reducing the cation-solvent interaction is crucial to inhibit electrolyte decomposition, suppress [Li-solvents]$^+$ co-intercalation behavior in LIBs, and improve the oxidative stability.[22] The Li^+-solvent interactions observed in WSE exhibit similarities to those of HCE. However, the distinct Li^+ solvation environment in WSE leads to different chemical properties of SEI. Several studies have demonstrated that the formation of weakly solvated complexes lowers the migration energy barriers of lithium ions, enabling Li^+ to migrate more freely in the solvent and undergo desolvation more easily, thereby improving the rate capability. In addition, the stability of solvent complexes affects the cycle and safety performance of batteries. Therefore, understanding the functional interactions between cations and solvents is requisite for optimizing the electrolyte composition of lithium batteries.

The extremely weak lithium-solvent interaction in WSEs enables Li^+ to easily desolvate as well as lithiation with the electrode materials. However, some WSEs struggle to match high mass loading electrodes due to the poor ionic conductivity. By removing DME from the conventional 1 M LiFSI DOL/DME electrolyte, the cation–anion interaction is enhanced in the solvation structure, increasing the ratio of CIP and AGG (**Figure 12a–f**), and enabling effective compatibility with high mass loading graphite anodes.[103] The CE of LMB is highly correlated with the morphology of plated lithium during the charging process, with respect to fluorinated solvents, which weakly solvate Li^+, tend to plate bulk lithium particles with higher CE. This could be attributed to the weak solvation of Li^+, leading to an increase in the exchange current density (j^0), altering the Li/Li^+ equilibrium potential. Additionally, the WSE exhibited a positive surface charge density, consequently reducing surface charge fluctuations and increasing surface energy.[104,105] This behavior thermodynamically favors homogeneous lithium plating[24] that is more pronounced in fluoride-containing WSEs.

In polyethylene oxide-based solid polymer electrolytes, due to the special coordination of ethylene oxide groups, there is an overly strong interaction between Li^+ and the electrolyte, hence, it is difficult for Li^+ to dissociate.[106–108] By converting volatile solvents into solid polyacetal electrolytes, retaining weak solvation properties, its asymmetric structure leads to a unique twisted helical solvation sheath, effectively mitigating overly strong Li^+-electrolyte interactions. Additionally, this modulates the dissociation and desolvation kinetics of Li^+ to

© 2025 The Author(s). Advanced Energy Materials published by Wiley-VCH GmbH

16146840, 0, Downloaded from https://advanced.onlinelibrary.wiley.com/doi/10.1002/aenm.202501272 by Karlsruher Institut Für Technologie, Wiley Online Library on [13/05/2025]. See the Terms and Conditions (https://onlinelibrary.wiley.com/terms-and-conditions) on Wiley Online Library for rules of use; OA articles are governed by the applicable Creative Commons License

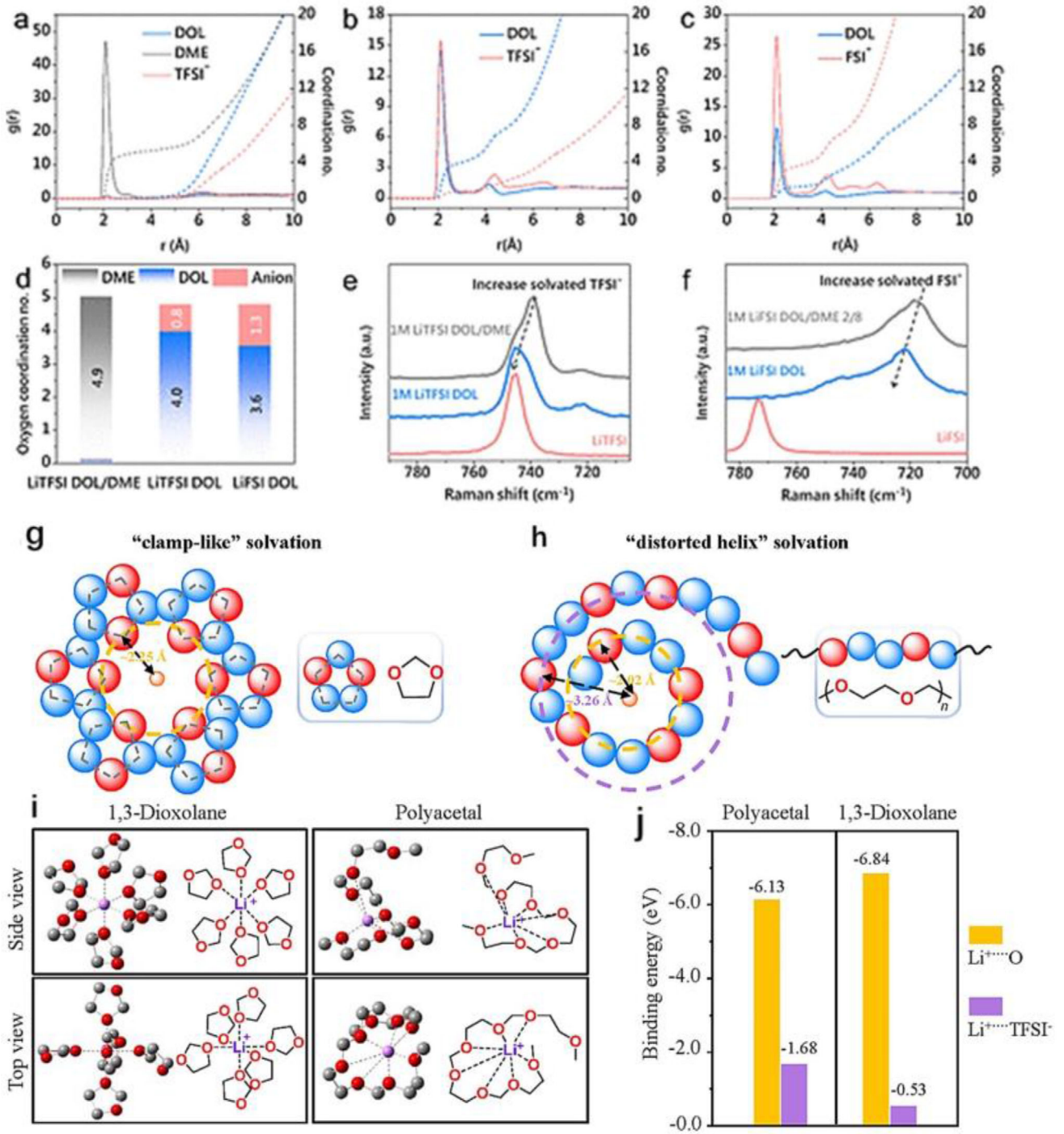

Figure 12. Solvation structures of different electrolytes. a–c) Li–O RDFs and the coordination number for various electrolytes. d) Oxygen coordination numbers with Li^+ in three electrolytes. e,f) Raman spectra of different salts, solvents, and electrolytes. Reproduced with permission.[103] Copyright 2023, American Chemical Society. g,h) Schematic illustration solvation structures of Li^+ in 1,3-dioxolane and Li^+ in polyacetal. i) Side and top view solvation structure of Li^+ in different solvents optimized by DFT. j) Binding energies of Li^+-O and Li^+-$TFSI^-$. Reproduced with permission.[109] Copyright 2023, Elsevier.

© 2025 The Author(s). Advanced Energy Materials published by Wiley-VCH GmbH

16146840, 0, Downloaded from https://advanced.onlinelibrary.wiley.com/doi/10.1002/aenm.202501272 by Karlsruher Institut Für Technologie, Wiley Online Library on [13/05/2025]. See the Terms and Conditions (https://onlinelibrary.wiley.com/terms-and-conditions) on Wiley Online Library for rules of use; OA articles are governed by the applicable Creative Commons License

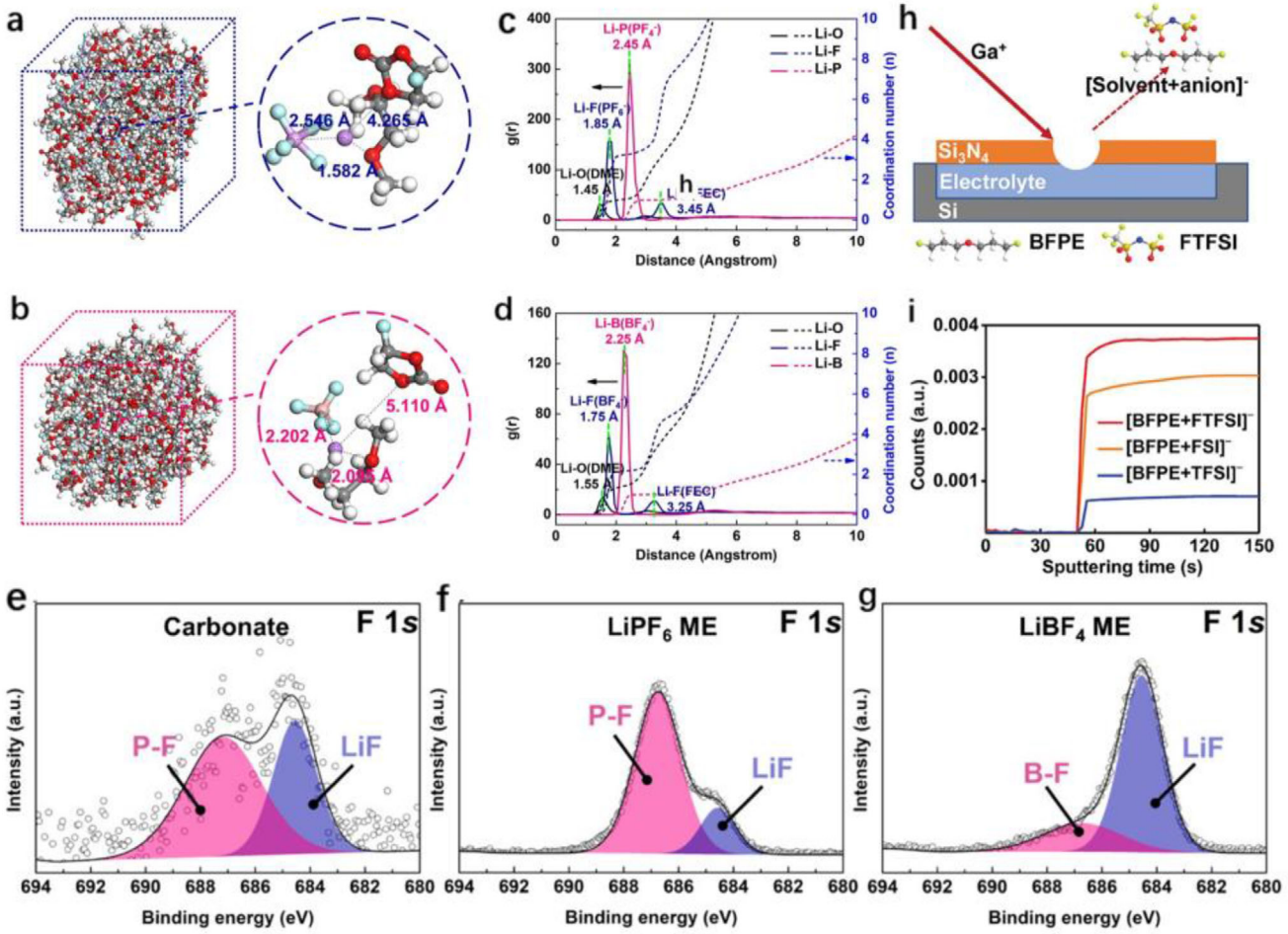

Figure 13. Analysis of electrolyte solvation structure. a, b) AIMD simulation snapshots and locally amplified solvation structure, and c, d) corresponding RDF and coordination number for various electrolytes. e–g) F 1s XPS spectra on the surface of deposited Li. Reproduced with permission.[47] Copyright 2023, John Wiley and Sons. h) Schematic setup of an in situ liquid SIMS cell. i) Depth profiles of 0.5 M LiFSI/0.5 M LiFTFSI/0.5 M LiTFSI in BFPE electrolytes. Reproduced with permission.[111] Copyright 2023, John Wiley and Sons.

varying degrees (Figure 12g–j). This newly developed weakly solvated polymer electrolyte, regulated by its aggregate structure, exhibits excellent rate performance and stable cycling ability.[109]

3.2.2. Solvents and Anions

Enhancing the strength of Li^+-anion coordination is another way to construct WSEs in addition to using WSS. By comparing the solvation structures formed by various lithium salts in DME, the relationship between the dissociation degree of lithium salts and the solvation structure was investigated. In the case of DME paired with FEC, which exhibits the lowest dissociation degree of $LiBF_4$ constituting the WSE, the relatively low binding energy of Li^+-BF_4-DME (0.65 eV) facilitates easier desolvation of BF_4^- and its preferential participation in the interphase formation. Ab initio molecular dynamics (AIMD) simulations have revealed that the Li^+-FEC distance is considerably larger compared to that of Li^+-DME and Li^+-anion, indicating that FEC has a minor impact on the solvated structure (**Figure** 13a-d). However, its incorporation contributes to the formation of a stable interphase between Li anode and $LiCoO_2$ cathode, as well as the formation of highly ionic-conductive anion-driven CEI in this electrolyte. The decomposition of the BF_4^- anion, resulting in the generation of LiF in large quantities, promotes the uniform deposition of Li^+ on the lithium anode (Figure 13e-g). Meanwhile, the electrolyte effectively preserves the structural stability and enhances the stability of the $LiCoO_2$ cathode at high voltage.[47]

The solvation sheath of Li^+ is composed of both solvent and anions. However, due to the weak association ability between solvent molecules and lithium ions in WSE, the loose structure of the solvent molecular layer not only facilitates the desolvation of cations but also allows anions to easily dissociate from the solvent environment. This enhances the electrostatic attraction between anions and the electrode surface, promoting the formation of a stable adsorption layer of anions on the electrode surface.[110] To understand anion-solvent interactions, three conventional anions, $TFSI^-$, FSI^- and asymmetric (fluorosulfonyl) (trifluoromethanesulfonyl)imide ($FTFSI^-$) were selected. The use of bis(3-fluoropropyl) ether (BFPE), a solvent with weak Li^+

© 2025 The Author(s). Advanced Energy Materials published by Wiley-VCH GmbH

16146840, 0, Downloaded from https://advanced.onlinelibrary.wiley.com/doi/10.1002/aenm.202501272 by Karlsruher Institut Für Technologie, Wiley Online Library on [13/05/2025]. See the Terms and Conditions (https://onlinelibrary.wiley.com/terms-and-conditions) on Wiley Online Library for rules of use; OA articles are governed by the applicable Creative Commons License

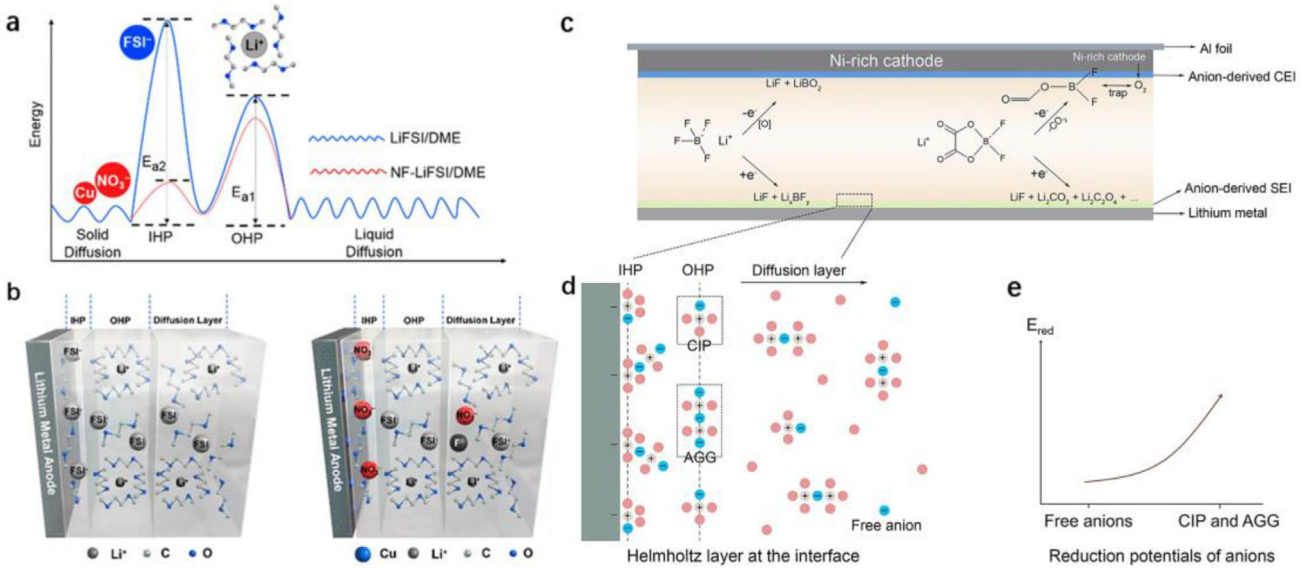

Figure 14. a) The relationship between the energy barrier of Li^+ and the specific adsorption in the IHP and OHP. b) Schematic diagram of the migration process of solvated Li^+. Reproduced with permission.[112] Copyright 2019, American Chemical Society. Schematic illustration of c) anion-enrichment interphase and anion-derived electrode-electrolyte interphases and d) electrode interphase. e) Reduction potentials of free anions, CIP, and AGG. Reproduced with permission.[26] Copyright 2023, Springer Nature.

interaction, made the interaction of anions-solvents more pronounced. The interaction of anions-solvents was verified by in-situ liquid secondary ion mass spectrometry (SIMS), which demonstrated the existence of [BFPE-TFSI] and [BFPE-FSI]. (**Figure** 13h,i). Ultimately, it revealed that the 1.5 M LiFTFSI-BFPE electrolyte with stronger interaction of anion-solvent is capable of achieving superior cycling performance.[111]

The solvated cations initially reside within the solvated sheath layer and are then transported to the electrode surface. Within this process, the Li^+ solvated sheath migrates towards the bilayers, specifically the outer Helmholtz plane (OHP) and the inner Helmholtz plane (IHP). Given that the thickness of the inner layer of the IHP is smaller than that of Li^+ solvated sheaths, only a single ion or solvent molecule exists within the IHP. Upon entering the OHP, the Li^+ solvated sheath undergoes Li^+ desolvation, and finally adsorbs onto the surface of the electrode or enters the bulk of the electrode (Figure 14a and b).[5,112–114] The design of the WSE necessitates an increased presence of anions within the IHP, outcompeting the solvent, and finally decomposing on the surface of the electrode to form the SEI layer. With the introduction of an F group, a fluorinated linear carboxylate (tFEP) precisely modulated the solvated structure, forming an anion-rich interphase in the WSE. This facilitates greater anion decomposition within the IHP, fostering LiF-rich interfacial layer (Figure 14c–e), and suppressing detrimental reactions. The finally constructed anode-free pouch cell (>200 mAh) achieved a capacity retention of 80% after 100 cycles under harsh conditions.[26] In summary, the interaction mode between solvents and ions in WSEs exhibits a relatively loose solvation structure, which is conducive to enhancing the migration capability of Li^+ and reducing the viscosity of the electrolyte, thereby enhancing the electrochemical performance of the battery. However, this mode also requires careful regulation to ensure the formation of a stable SEI during battery operation.

3.3. The Effect of WSS on SEI Formation (Effect on Solvation Structure)

Most of the current theoretical simulation methods for electrolytes are based on molecular dynamics (MD) by constructing classical force fields and systems. Simulation of the internal molecular structure of the electrolyte offers further insight into the solvation structure. The RDF shows the distribution of each solvent molecule and anion in the Li^+ solvation sheath layer. Additionally, the number of ligands can be intuitively reflected in the solvent, the anion, and the coordination of Li^+.[115] DFT simulations can be utilized to determine the HOMO and LUMO energy level of each solvent and lithium salt. By comparing these values, one can, to some extent, infer the redox sequence of the components.[116] More accurately, this comparison reflects the potential at which the electrolyte undergoes reduction under negative potentials and the potential at which the solvent experiences oxidation under positive potentials.[117] In the design of electrolytes for LMB, many researchers have introduced solvents/lithium salts with lower LUMO energy. This allows them to undergo preferential reduction and decomposition into favorable components on the LMA, which guarantees a robust SEI.[118] The thin inorganic-rich SEI can reduce the resistance and activation energy of Li^+.[119] Conventional electrolytes rely on carbonate-based solvent decomposition to form the SEI due to the use of strongly solvating solvents. In this type of solvent-based electrolyte, anions and Li^+ have difficulty in coordinating, leading to the predominant formation of solvent-derived organic-rich interfacial layers. In situ electrochemical atomic force microscopy (AFM) demonstrates that the formation of LiFSI-derived inorganic SEI in the WSE (1.0 M LiFSI dissolved in 1,4-DX) follows a hybrid two- or three-dimension (2D/3D) growth mode. Additionally, the nucleation model transitions from 3D planar[120,121] to 2D island[122–125] with increasing

© 2025 The Author(s). Advanced Energy Materials published by Wiley-VCH GmbH

16146840, 0, Downloaded from https://advanced.onlinelibrary.wiley.com/doi/10.1002/aenm.202501272 by Karlsruher Institut Für Technologie, Wiley Online Library on [13/05/2025]. See the Terms and Conditions (https://onlinelibrary.wiley.com/terms-and-conditions) on Wiley Online Library for rules of use; OA articles are governed by the applicable Creative Commons License

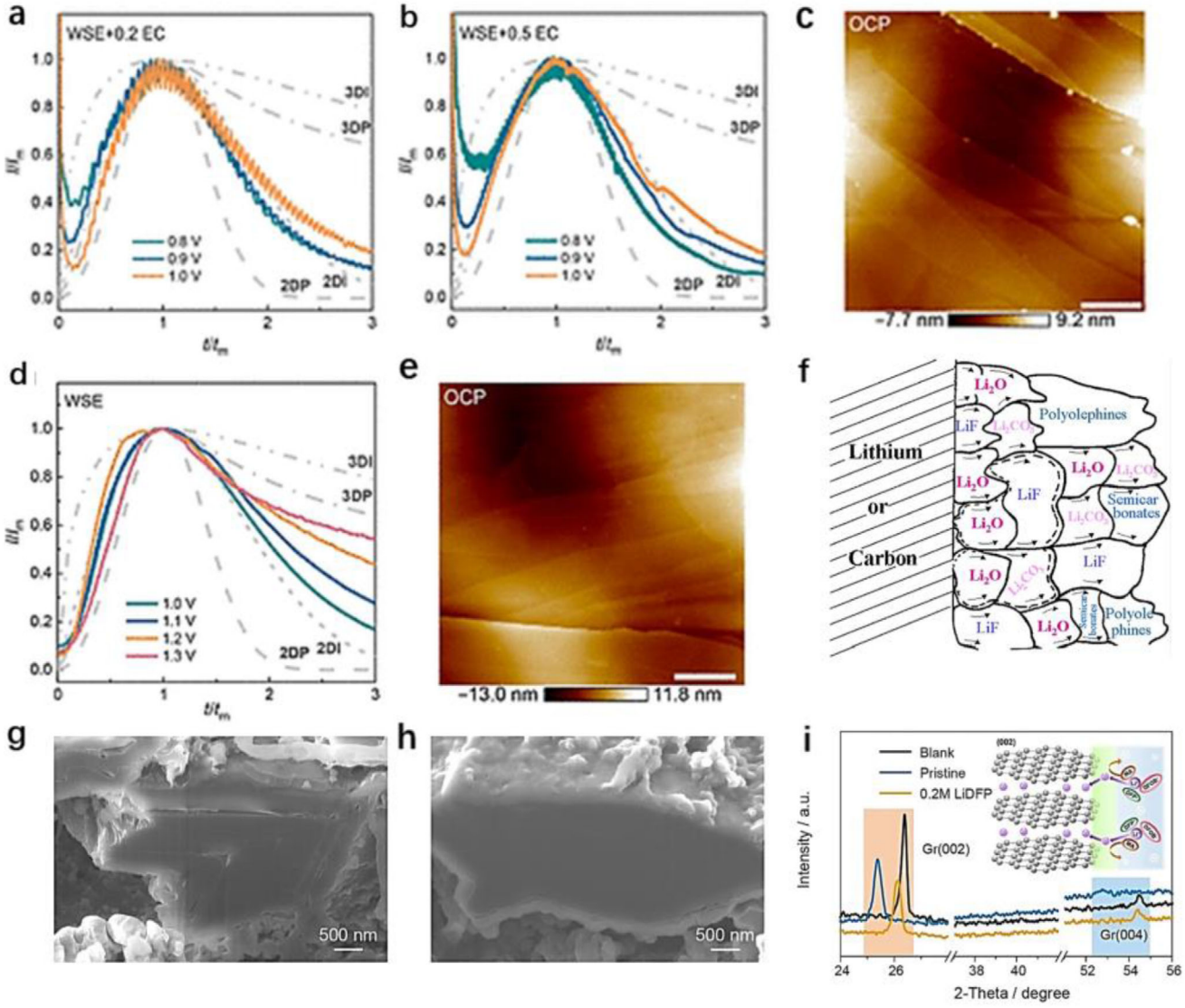

Figure 15. a, b) Dimensionless current–time transients at various potentials in comparison with the classical 2D and 3D nucleation models. In situ AFM images of the HOPG electrode at c) OCP. d, e) In situ monitoring of the nucleation and growth of a LiFSI-derived inorganic SEI on a HOPG electrode. Reproduced with permission.[126] Copyright 2023, American Chemical Society. f) Schematic illustration of SEI components. Reproduced with permission.[127,132] Copyright 2017, IOP Publishing. FIB-SEM images of the Gr anode in g) pristine and h) LiDFP-modified electrolyte after 1 cycle at −20 °C, and i) the corresponding XRD spectra. Reproduced with permission.[134] Copyright 2023, John Wiley and Sons.

overpotential (**Figure 15**d, e). Conversely, the SEI derived from EC in conventional electrolytes follows the 2D island nucleation and growth mode (Figure 15a–c).[126]

One of the popular models of SEI is the "mosaic model" proposed by Peled et al. in 1997[127] (Figure 15f), which suggests that multiple SEI components are formed simultaneously. The inner layer comprises an inorganic component with complete salt decomposition, while the outer layer consists of more organic components. The organic-dominated outer layer of the SEI is a porous structure that can retain some of the electrolyte and enhance the conductivity of Li^+.[128,129] Therefore, the SEI swells upon contact with the electrolyte, and this swelling behavior depends on the composition of the electrolyte. Conversely, the extent of swelling impacts the available amount of electrolyte in the cell and influences the cycling lifetime.[130,131]

The mechanical properties of the SEI were observed by in situ AFM, revealing that lithium deposition preferentially occurs in the thinner regions of SEI, and a uniform SEI inhibits dendrite growth. Shen et al.[133] concluded that the stability is optimal when the elastic modulus of the SEI exceeds 3 GPa. Liang et al.[134] developed a new SEI by introducing an organic-anion-rich primary solvation sheath (PSS) layer into the WSE. This was achieved by introducing an inorganic difluorophosphate anion (DFP^-) to partially replace $DFOB^-$. The DFP^- priority participates in the formation of SEI, generates a Li_3PO_4-rich homogeneous SEI structure while keeping the weak solvation ability of the electrolyte. This effectively inhibits solvent co-intercalation

© 2025 The Author(s). Advanced Energy Materials published by Wiley-VCH GmbH

16146840, 0, Downloaded from https://advanced.onlinelibrary.wiley.com/doi/10.1002/aenm.202501272 by Karlsruher Institut Für Technologie, Wiley Online Library on [13/05/2025]. See the Terms and Conditions (https://onlinelibrary.wiley.com/terms-and-conditions) on Wiley Online Library for rules of use; OA articles are governed by the applicable Creative Commons License

and SEI expansion, regulates SEI formation chemistry at low temperatures (Figure 15g-i), and overcomes Li^+ solubility challenges at low temperatures, enabling stable, long-term cycling of the graphite-based anode.

The intricate reactions present within the cell mean it is still a significant challenge to examine the interphase structure of the SEI due to the lack of in situ operando detection techniques and computational methods that can fully describe the dynamic heterogenous passivation layer spatially and temporally. In the electrolyte, WSS forms solvation structures with lithium salts and other components. The formation of these solvation structures affects the solubility, ion migration rate, and stability of the electrolyte. Several studies have demonstrated that the incorporation of WSS can improve the dissolution kinetics and electrode/electrolyte interfacial stability, thereby improving the power density and cycle life of the cell.

3.4. WSE Performance at Low Temperature

The inhomogeneous lithium deposition and the sluggish ion movement at sub-zero temperatures often lead to serious capacity loss and premature failure. Commercial lithium batteries exhibit a capacity retention of only 12% at −40 °C compared to that of room temperature.[135] Moreover, commercial EC-based electrolytes begin to freeze at around 5 °C, rendering them ineffective for use in low-temperature environments. Lately, researchers have focused on electrolytes that enable stable cycling at low temperature. The electrolyte should possess a wide temperature range, ensuring excellent Li^+ diffusion kinetics even at sub-zero temperatures,[136,137] and maintaining good charge/discharge CE. The high electrochemical performance is closely linked to the solvation structure. At sub-zero temperatures, efficient charging relies heavily on weak solvation kinetics. Conventional electrolytes with high dielectric constant solvents facilitate full dissociation of lithium salts, ensuring the conductivity of ions. However, their strong affinity also inhibits the desolvation kinetics on the electrode surface.[138,139] HCE applied at low temperature significantly increases the viscosity, potentially leading to salt precipitation, which fails to address the challenge of poor performance at low temperature.[13] Ideal low-temperature electrolytes should possess high ionic conductivity, chemical stability, and a weak coordination ability with lithium ions to improve Li^+ transfer kinetics at low temperature. Recent research based on WSE demonstrated that the WSS facilitates the desolvation process at low temperature.[140]

The desolvation energy of lithium ions in solvents depends on the coordination ability and coordination number of solvent molecules in the Li^+ solvation sheath, which is closely correlated with the number of solvents and anions in the solvation structure. Choosing solvents with low solvation ability can adjust the electrolyte solvation structure and promote the desolvation ability of Li^+, thus accelerating the desolvation process. This enables Li to keep outstanding deposition kinetics at low temperatures.[141,142] DMM, characterized by its weak solvating properties, tends to form less stable four-membered ring structure complexes with lithium ions, exhibiting weaker interaction compared to DME-Li^+. MD simulations demonstrated that in electrolytes prepared with DMM, the primary solvated sheath is mainly composed of Li-O interactions with FSI^- (**Figure 16**a,b). This suggests that Li^+ prefers to coordinate with anions, which is also supported by Raman and NMR characterization.[43] Its rapid desolvation process enables LMB to obtain uniform lithium deposition at −40 °C. The Li||SPAN full cell exhibits high initial capacity and good capacity retention after 120 cycles (Figure 16c,d). Liang et al.[44] utilized low-affinity solvents in synergistic cooperation with anions. They optimized a cyclic ether-based electrolyte containing 1 M $LiBF_4$ dissolved in DOL and THF to design the electrolyte with a weakly solvated structure that promotes overall reaction kinetics. The design allows the Li||CF_x battery to operate at very low temperatures of -40 °C, -60 °C, and -80 °C (Figure 16e–g).

Similarly, in graphite anodes, the lower operating potential during Li-ion intercalation in graphite results in a narrow range of voltage fluctuations, which is a primary cause of irreversible losses and capacity degradation.[143–145] This issue becomes more pronounced when operating at low temperature, which further constrains the practical application of LIBs in a cold environment. WSS, like ETFA, when paired with film-forming co-solvent FEC in WSE, effectively resolves this issue by achieving high ionic conductivity across a wide temperature range. It was found that the thickness of the SEI gradually decreases as the temperature reduces (Figure 16h–j), thereby shortening the diffusion path of Li^+ and facilitating their rapid transfer at the electrode/electrolyte interphase. This enables fast desolvation of lithium ions even under the harsh conditions of low temperature and high rate, allowing the Graphite||LFP full cell to cycle normally at −60 °C.[146]

In order to obtain a superior capacity retention of graphite-based lithium batteries at low temperature, researchers have adopted the method of charging at room temperature to enhance the discharge performance at low temperatures, ignoring the increase of charge transfer resistance (R_{ct}).[96,147,148] While Nan et al.[149] emphasized the importance of weak ionic dipole interactions between solvent molecules and lithium ions for reducing R_{ct}. They developed a low-polarity solvent electrolyte using ethyl methyl carbonate (EMC) with a wide temperature range and small dipole moment (μ = 0.89 D), paired with TTE, which exhibits weaker ionic dipole interaction with lithium ions compared to high-polar solvents. This approach effectively reduces the activation energy and resistance during charge transfer, thereby enhancing the transport kinetics. The Graphite||NCM811 full cell exhibits a significantly smaller increase in impedance and a simultaneous decrease in charge-transfer activation energy with this electrolyte (Figure 16k–n). This contributed to more than 80% capacity retention of the full cell at both −30 and −40 °C, along with free lithium plating during cycling.

The impact of ions in the electrolyte on the design of wide-temperature-range electrolytes is multifaceted, with ion transport rate being a crucial factor. To achieve a stable ionic transport process in the electrolyte at low temperatures, fluorinated solvents and specific anions can be introduced to participate in the solvation coordination. The electrolyte was prepared by combining a fluorinated solvent and non-polar tetrafluoro-1-(2,2,2-trifluoromethoxy)ethane (D2), which has a low relative dielectric constant. The combination of D2 remarkably reduced the viscosity of the electrolyte and suppressed the solidification of the

© 2025 The Author(s). Advanced Energy Materials published by Wiley-VCH GmbH

16146840, 0, Downloaded from https://advanced.onlinelibrary.wiley.com/doi/10.1002/aenm.202501272 by Karlsruher Institut Für Technologie, Wiley Online Library on [13/05/2025]. See the Terms and Conditions (https://onlinelibrary.wiley.com/terms-and-conditions) on Wiley Online Library for rules of use; OA articles are governed by the applicable Creative Commons License

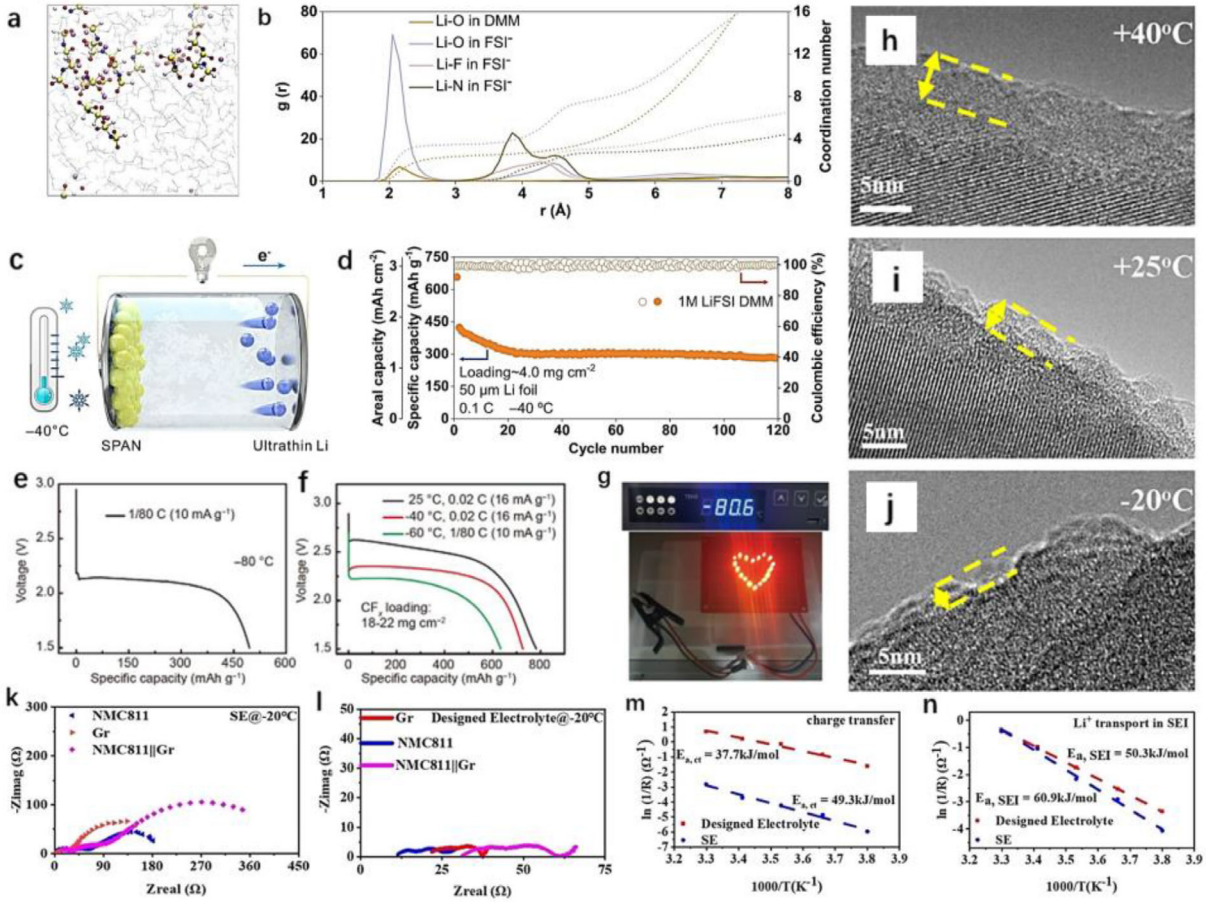

Figure 16. a) MD simulation snapshots and corresponding b) RDF of the 1 M LiFSI DMM electrolyte. c) Schematic diagram of the Li||SPAN full cell and d) its long-cycle performance. Reproduced with permission.[43] Copyright 2022, John Wiley and Sons. e-g) Low-temperature performance realized by high-loading CF_x. Reproduced with permission.[44] Copyright 2023, Springer Nature. h-j) TEM images of graphite electrodes. Reproduced with permission.[146] Copyright 2022, John Wiley and Sons. k,l) EIS spectra of the Gr||NMC811 with different electrolyte. Activation energies of m) the charge transfer process and n) Li^+ transport in the SEI of the graphite. Reproduced with permission.[149] Copyright 2022, John Wiley and Sons.

electrolyte, ensuring the ion transmission rate. The use of fluorinated solvents reduces the inherent desolvation force of Li^+, which can remarkably alleviate the relationship between solvent/Li^+/anion, and reduce the strong interactions between Li^+ and the solvent dipole.[150]

4. WSE for Post-Lithium Batteries

WSE has also been applied in other energy storage fields beyond LIBs, including alkaline-secondary batteries, fuel cells, and capacitors. Currently, research on WSE for use in post-lithium batteries is an emerging area of interest owing to the favorable structuring, dynamics, and properties offered by these media. Therefore, we provide an overview of the research and latest developments of WSE in zinc batteries, sodium batteries, and potassium batteries.

4.1. WSE for Zinc Batteries

The initial development of zinc batteries dates back to the early 19th century, preceding the development of lithium batteries around the 1960s. However, zinc batteries faced challenges such as low energy density, relatively high self-discharge rate, and slow charging speed, which limited their commercialization. With ongoing research, attention shifted towards aqueous zinc batteries (AZBs).

AZBs have aroused significant concern because of their high ionic conductivity, non-toxicity, non-flammability, high volume/weight specific capacity (5855 mAh cm^{-3}, 820 mAh g^{-1}), and the relatively low redox potential of the zinc anode.[154–157] However, practical applications have been impeded by challenges such as dendritic growth on the zinc anode and parasitic reactions.[158] To address these limitations, Hu and colleagues explored a weakly solvated colloid electrolyte for aqueous zinc-metal batteries (AZMB), utilizing $NaErF_4$@$NaYF_4$ nanocrystals as electrolyte additives. This strategy entails the preferential adsorption of functional metal ions, which creates an electrostatic shielding layer to suppress dendritic growth. Simultaneously, released fluoride ions participate in forming an interphase layer rich in ZnF_2 to optimize the electrode/electrolyte interphase (**Figure 17**a). This significantly promotes the Zn^{2+} desolvation process, leading to stable cycling for 2100 h in a symmetrical cell (Figure 17b). The

© 2025 The Author(s). Advanced Energy Materials published by Wiley-VCH GmbH

16146840, 0, Downloaded from https://advanced.onlinelibrary.wiley.com/doi/10.1002/aenm.202501272 by Karlsruher Institut Für Technologie, Wiley Online Library on [13/05/2025]. See the Terms and Conditions (https://onlinelibrary.wiley.com/terms-and-conditions) on Wiley Online Library for rules of use; OA articles are governed by the applicable Creative Commons License

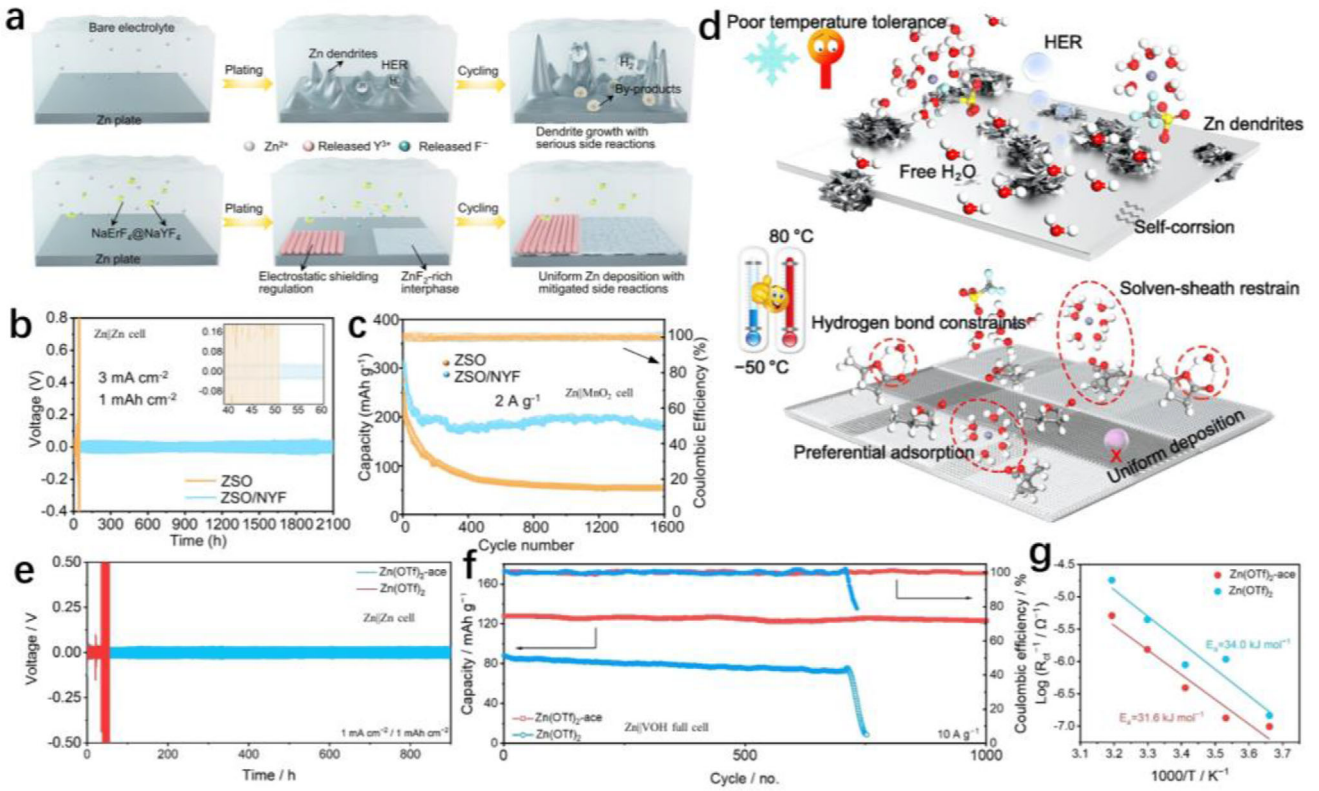

Figure 17. a) Schematic illustrations of the sustained-release effect and working mechanism of the $NaErF_4$@$NaYF_4$ additive. b) Voltage profiles and c) Long-term cycling performance of different electrolytes; Reproduced with permission.[151] Copyright 2023, American Chemical Society. d) Schematic diagram of zinc metal anode in (up) pristine aqueous electrolyte and (down) hybrid electrolyte with c-valerolactone; Reproduced with permission.[152] Copyright 2023, Elsevier B.V. e) Long-term stripping/plating behavior, f) galvanostatic cycling performance, and g) Arrhenius curves and comparison of activation energies of Zn plate in different electrolyte; Reproduced with permission.[153] Copyright 2023, John Wiley & Sons.

assembled Zn||MnO_2 full cell exhibits stable cycling for 1600 cycles (Figure 17c). Additionally, the addition of γ-butyrolactone to aqueous WSEs can inhibit dendrite growth, ensuring the normal operation of AZMB over a wide temperature range (−97 to 80 °C).[152] The comparison of the interaction mechanisms of different electrolytes on the anode surface is illustrated in Figure 17d. In the original aqueous electrolyte, the free water molecules make the zinc anode susceptible to dendritic growth, corrosion, and hydrogen evolution reactions, resulting in poor temperature resistance. In contrast, the developed hybrid electrolyte exhibits better stability due to its reduced water molecules and optimized regulation of nucleation and zinc growth. This improvement increases the adaptability of the battery to extreme temperatures.

Similar challenges exist in aqueous zinc-ion batteries (AZIB). Reports suggest that introducing acetone with a low dielectric constant can be employed to formulate a new type of aqueous electrolyte to address such issues. This water-soluble electrolyte is represented by $Zn(OTf)_2$-ace, consists of 1 M $Zn(OTf)_2$ (Zinc trifluoromethanesulfonate) and 50 v/v% acetone, achieving a weakly solvating structure for Zn^{2+} in H_2O.[153] This structure effectively mitigates side reactions related to the solvation of H_2O and promotes the desolvation process to inhibit dendritic growth. This strategy extends the cycle life of Zn||Cu asymmetric cells from 30 h to over 800 h (Figure 17e). The Zn||$V_2O_5{\cdot}nH_2O$ full cell exhibits exceptional cycling stability, with a capacity retention of 95.9% after 1000 cycles (Figure 17f). This is attributed to the reduced desolvation energy of $Zn(OTf)_2$-ace (Figure 17g).

4.2. WSE for Sodium Batteries

The development of sodium batteries commenced around the 1970s, benefiting from the widespread geographical distribution of sodium sources,[159] high compatibility, and good safety. Sodium batteries are considered to be at the forefront of alternative energy storage technologies following LIBs.

In practical applications, the sodium metal anode often undergoes side reactions with the electrolyte, leading to the formation of an unstable SEI layer accompanied by the growth of sodium dendrites.[160] Additionally, during the sodium plating/stripping process, sodium dendrites are prone to fracture and detach, converting to "dead sodium" and causing the failure of the battery.[161,162] The simplest way to address these issues is by adjusting the electrolyte composition to construct a stable SEI/CEI layer.[163–166] Zheng et al. developed an electrolyte with lower solvent affinity, namely 0.8 M $NaPF_6$-FEC/EMC/HFE (volume ratio 3:3:4; HFE: 1,1,2,2-tetrafluoroethyl 2,2,3,3-tetrafluoropropyl ether).[20] The electrolyte facilitates sodium metal batteries (SMBs) to exhibit improved rate capability and low-temperature

© 2025 The Author(s). Advanced Energy Materials published by Wiley-VCH GmbH

16146840, 0, Downloaded from https://advanced.onlinelibrary.wiley.com/doi/10.1002/aenm.202501272 by Karlsruher Institut Für Technologie, Wiley Online Library on [13/05/2025]. See the Terms and Conditions (https://onlinelibrary.wiley.com/terms-and-conditions) on Wiley Online Library for rules of use; OA articles are governed by the applicable Creative Commons License

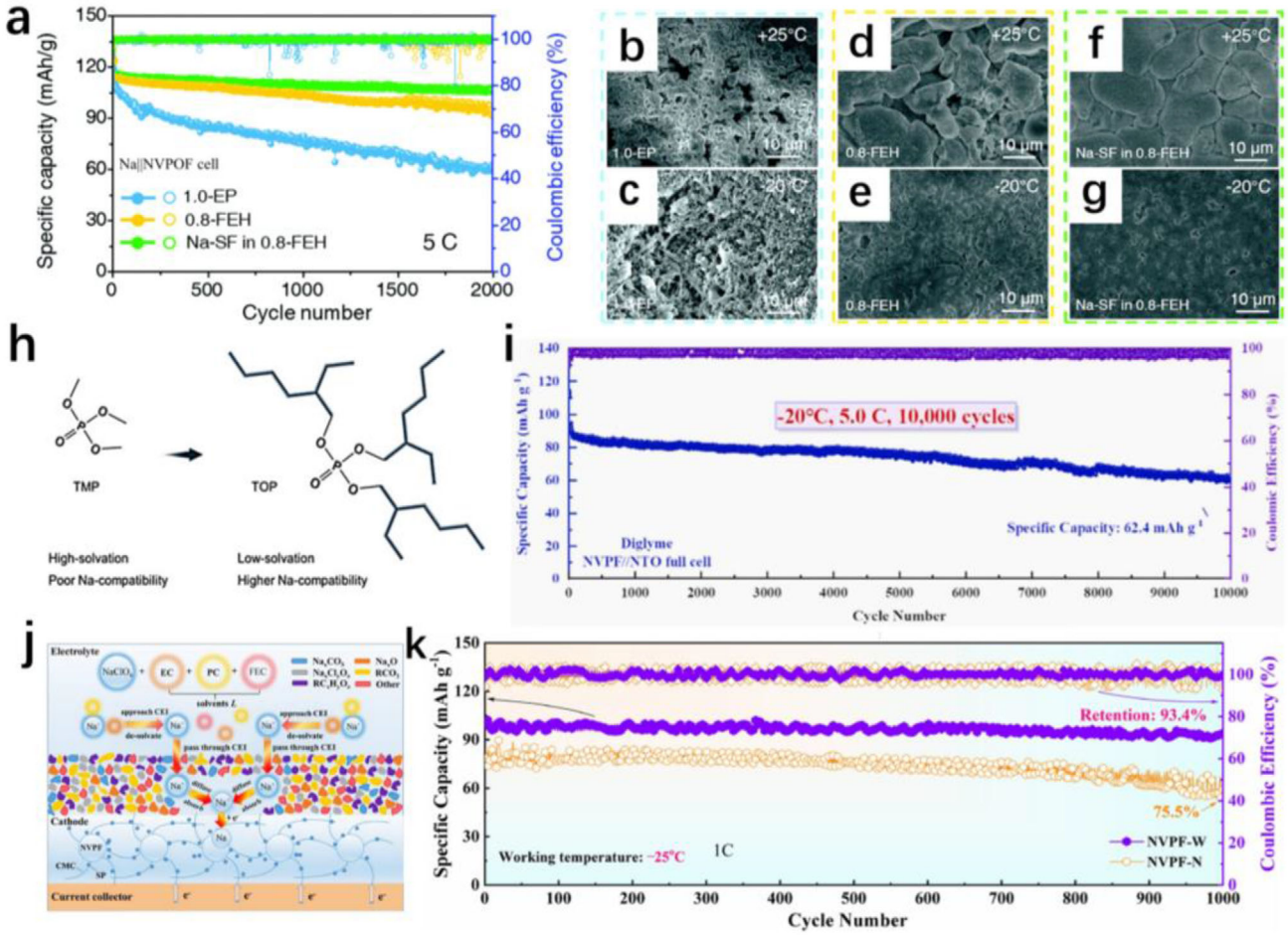

Figure 18. a) Cycling performance of various electrolytes. SEM images showing deposition morphology with bare Na in b, c) 1.0-EP and d) and e) 0.8-FEH electrolytes, and f, g) Na-SF anode in the 0.8-FEH electrolyte; Reproduced with permission.[20] Copyright 2021, Royal Society of Chemistry. h) Molecular structures of TMP and TOP solvents. Copyright 2023, John Wiley & Sons; Reproduced with permission.[27] i) Cycle performance of SIBs; Reproduced with permission.[168] Copyright 2022, Elsevier B.V. j) Schematic illustration of the NVPF/interphase/electrolyte system in the WSE. k) long-term cycling performance of the NVPF cathodes; Reproduced with permission.[21] Copyright 2021, Elsevier B.V.

performance. Under the condition of high rate of 5C, the Na||$Na_3V_2(PO_4)_2O_2F$ (NVPOF) cell obtains stable cycling for 2000 cycles with 92.4% capacity retention (**Figure 18a**). At the same time, it significantly improves the deposition morphology of Na-SF (SnF_2-treated Na) anode (Figure 18b–g). Recent developments in sodium batteries have achieved a significant breakthrough in enabling fast charging capabilities in extreme environments. This advancement was made possible by incorporating a weakly solvating co-solvent THF, into DME. As a result, SMBs demonstrated an exceptional high-rate performance, even under low-temperature conditions. The electrolyte formed a sodium fluoride (NaF)-rich SEI layer on the surface of the sodium electrode, suppressing dendrite growth and ensuring stable cycling of SMBs at −60 °C.[167]

Furthermore, by adjusting the molecular structure of tri-(2-ethylhexyl) phosphate (TOP), a WSE (1.2 M NaTFSI/DEC-FEC-TOP) with non-flammability and high stability for sodium-metal batteries has been successfully developed.[27] The key design principle is extending the phosphate framework through the —CH_2 group and incorporating this into the traditional carbonate electrolyte (Figure 18h). With the molecular volume increase, the solvating ability of the TOP solvent reduces. This molecularly tuned electrolyte not only exhibits good compatibility with metallic sodium but also achieves lower SEI dissolution rates at both room temperature and high temperature.

To promote the development of stable and high-energy sodium-ion batteries (SIBs), electrolytes yielding optimized interphases at both the electrodes are of paramount importance[169,170] The design of WSEs to suppress SEI dissolution can be divided into the following aspects: selecting solvents with appropriate polarity, regulating the ion-solvent structure to decrease the amount of free solvent molecules, and adjusting the SEI construction to promote the formation of low solubility SEI components.[23] Zheng and colleagues modified the composition of the electrolyte system in consideration of the concentration factor, proposed a weak solvation strategy, and significantly improved the cycling performance of polyanion-type $Na_3V_2(PO_4)_2F_3$ (NVPF) positive electrode material.[168] Noting that the low-concentration DGME (diethylene glycol dimethyl ether)-based electrolyte exhibits high adaptability to low-temperature SIBs. Upon further analysis, they

© 2025 The Author(s). Advanced Energy Materials published by Wiley-VCH GmbH

16146840, 0, Downloaded from https://advanced.onlinelibrary.wiley.com/doi/10.1002/aenm.202501272 by Karlsruher Institut Für Technologie, Wiley Online Library on [13/05/2025]. See the Terms and Conditions (https://onlinelibrary.wiley.com/terms-and-conditions) on Wiley Online Library for rules of use; OA articles are governed by the applicable Creative Commons License

discovered that the weakly solvating structure of Na^+-DGME was conducive to accelerating Na^+ diffusion and significantly reducing the interfacial charge transfer energy. Even at −20 °C, the $Na_2Ti_2O_5$||NVPF full cell assembled with this WSE could achieve stable cycling for 10000 cycles at a high rate of 5C (Figure 18i). Additionally, a feasible strategy involves employing WSE for simultaneously tailoring the cathode/electrolyte interphase and refining the configuration of ion-solvent coordination structure in the electrolyte, thus diminishing the activation energy barrier associated with the charge transfer reactions.[21] The results indicate that a weakly solvating structure could spontaneously form when the electrolyte concentration was reduced to 0.3 M, with a lower binding energy. The schematic diagram of the electrode/electrolyte interphase in the WSE is shown in Figure 18j, where a dense and uniform CEI is formed on the surface of the cathode. The NVPF in WSE electrolyte exhibits a capacity retention of up to 93.4% after 1000 cycles at 1C (Figure 18k).

4.3. WSE for Potassium Batteries

The development of potassium batteries began around the 1980s. Due to their cost advantages, resource benefits, relatively high energy density, and low redox potential (0.1 V vs Li^+/Li), potassium batteries are highly competitive candidates for large-scale energy storage.[171–174]

Traditional ether-based electrolytes in potassium-ion batteries (PIBs) exhibit low polarization voltages. However, they face challenges such as ion-solvent co-intercalation into graphite anodes,[177] poor potassium metal plating properties, and limited oxidation stability. In addressing these challenges, Li and colleagues utilized DEE as an ether solvent to develop a WSE (1M KFSI-DEE, KFSI: potassium bis(fluorosulfonyl)imide).[22] The results indicate that when the cation-solvent interaction is strong, a [cation-solvent]$^+$ co-intercalation phenomenon occurs in the graphite anode. Conversely, when the interaction between cation-solvent is weak enough, the cation intercalation behavior can be observed. K||K symmetric cell using this WSE demonstrates a stable cycling within 1400 h (**Figure 19a**) and high oxidation stability up to 4.4 V, ascribed to the thinner and more uniform SEI layer (Figure 19b). Furthermore, simultaneously achieving the great compatibility with both anode and high-voltage cathode in the electrolyte is challenging in PIBs.[178] A dilute electrolyte (0.8 M) containing a fluorinated phosphate demonstrated great compatibility with the graphite anode and the high-voltage cathode.[80] The designed electrolyte, using triethyl phosphate (TEP) as the foundational molecule and replacing all hydrogen atoms on the terminal methyl group of TEP with fluorine atoms, finally synthesized the target of phosphoric TFP. The minimum ESP value indicates the solvent molecule's affinity with cations, which increased from −66.96 kcal mol^{-1} for TEP to −47.65 kcal mol^{-1} for TFP (Figure 19c). The TFP electrolyte exhibits a wider voltage stability window (>5 V) (Figure 19d). A robust SEI was formed on the graphite anode, as well as effectively inhibited the high-voltage induced corrosion of the Al current collector. Leveraging this WSE, the fluorophosphate vanadium potassium ($KVPO_4F$) cathode underwent stable cycling at an ultrahigh voltage (4.95 V) for 20 h (Figure 19e). While PIBs have achieved notable progress in cathode[179,180] and anode materials,[181] safety issues and poor long-term cycling stability are promoted by the use of highly flammable electrolytes and form an effective SEI.[182] Therefore, Fan et al. proposed a low-concentration, non-flammable, WSE of 1 M KFSI-FTEP (tris (2,2,2-trifluoroethyl) phosphate) (Figure 19f),[25] forming an anion-derived SEI even at low concentration. This electrolyte enables stable operation of K||Graphite cells for more than two years (Figure 19g), offering a novel insight for developing safe and high-performance electrolytes of PIBs. Furthermore, the PIBs with graphite anodes encounter volume expansion caused by the insertion of the K^+ large ion radius into the graphite electrode not only impacts the stability of electrode materials[22] but also contributes to the unstable SEI.[183] Replacement of graphite with hard carbon, which has more active sites, is a useful method for improving battery performance.[184] The insertion process of K ions into hard carbon involves a capacitance and diffusion mixed mechanism for K-ion storage, thereby reducing volume expansion to enhance structural stability.[185] Regarding solvent selection, there is a shift from linear ethers to cyclic ethers such as THF, known for its low polarity and low DN value. This weak solvent can not only suppress solvent co-intercalation but also regulate the dynamics of hard carbon through interphase chemistry, and form a thin, uniform inorganic-rich SEI.[175] The solvation structure is dominated by CIP and AGG (Figure 19h). HRTEM results reveal that, in contrast to the thickness range from 2 to 8.3 nm of SEI layer formed by EC-DMC electrolyte on carbon nanofiber, the SEI formed in THF-based electrolyte is thinner and more uniform, with a thickness of 4.5 nm (Figure 19i).

In potassium metal batteries, compared to traditional cell structures,[186] anode-free cells (Figure 19j) can avoid excessive use of potassium, thus approaching the theoretical energy density of the cell. However, at low temperature, the metal surface tends to form an unstable SEI and uncontrollable dendrite growth[187] thus, it is difficult to achieve highly reversible metal plating/stripping. Tang et al. designed a low-concentration of 0.4 M KPF_6-DME WSE and introduced polydimethylsiloxane (PDMS) capped with -OCH_3 groups as an additive to modify the potassium metal interphase.[176] In the electrolyte without PDMS, sharp cracks appeared due to the formation of an unstable SEI and the generation of "dead" potassium (Figure 19k). However, with the addition of PDMS, a stable and robust SEI layer formed in situ on the potassium metal surface, preventing dendrite formation (Figure 19l). This study accomplished highly reversible deposition of potassium in an anode-free potassium metal battery at −40 °C for the first time, providing valuable insights for related research on anode-free systems at low temperatures.

5. Conclusion and Outlook

In summary, WSEs exhibit limited solvation ability, giving rise to weak interactions with Li^+. This characteristic reduces the coordination of solvent with Li^+ and allows more anions to coordinate with Li^+, creating a solvation environment rich in CIPs and AGGs, similar to HCE and LHCE, yet at a conventional or low salt concentration. This structure promotes the generation of anion-derived interphase, reduces the desolvation energy barrier, and improves the kinetics of lithium plating. Moreover, WSE overcomes the limitations of HCE, i.e., high viscosity, low ionic

© 2025 The Author(s). Advanced Energy Materials published by Wiley-VCH GmbH

16146840, 0, Downloaded from https://advanced.onlinelibrary.wiley.com/doi/10.1002/aenm.202501272 by Karlsruher Institut Für Technologie, Wiley Online Library on [13/05/2025]. See the Terms and Conditions (https://onlinelibrary.wiley.com/terms-and-conditions) on Wiley Online Library for rules of use; OA articles are governed by the applicable Creative Commons License

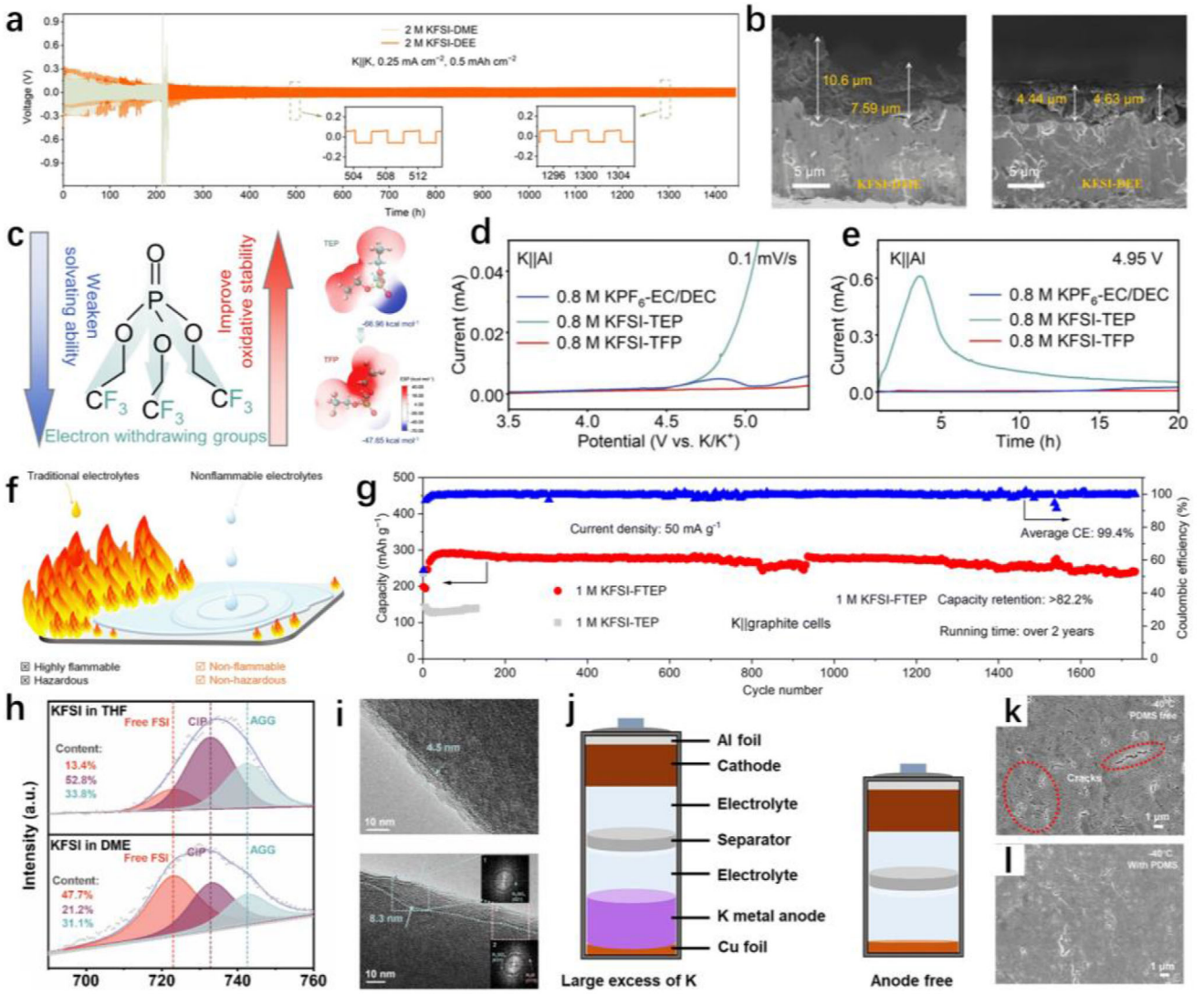

Figure 19. a) Long-term cycling and b) SEM images of a cross-section of Cu electrodes in different electrolytes; Reproduced with permission.[22] Copyright 2022, John Wiley & Sons. c) Molecular structure, its design principles, and ESP results of different solvents. d) LSV curves and e) leakage currents collected from CA tests of various electrolytes; Reproduced with permission.[80] Copyright 2023, John Wiley & Sons. f) Flammability diagram of traditional and non-flammable electrolytes. g) CE and cycle stability of the two different electrolytes; Reproduced with permission.[25] Copyright 2023, Royal Society of Chemistry. h) Raman spectra and i) TEM images of third-cycled CNFs with different electrolyte; Reproduced with permission.[175] Copyright 2022, Elsevier B.V. j) Schematic illustration of the conventional K metal battery and anode-free battery. SEM images of the K deposit layer on Cu with k) KPF_6-DME and l) KDP electrolyte; Reproduced with permission.[176] Copyright 2023, Springer Nature Limited.

conductivity, and poor performance across a wide temperature range. As a result, WSEs are anticipated to improve the low-temperature and fast-charging performance of batteries. The selection of WSS is paramount in the design of WSE. The fundamental design principle of WSS is to regulate and balance the interactions between the Li^+-solvent molecules and the Li^+-anions. Ether-based solvents are currently the most studied, followed by fluorinated solvents, silicone-based solvents, and specially designed solvents, all of which show considerable potential. In terms of lithium salts and additives, they have been comparatively less investigated, with a focus primarily on low-dissociation salts. The low viscosity, suitable ionic conductivity, and broad ESW of WSE have increased their utilization in lithium batteries and other energy storage areas. These applications include emerging post-lithium batteries such as zinc, sodium, and potassium batteries. It is worth noting that although WSEs offer unique advantages and have demonstrated promising results in improving battery performance, they also face limitations that must be resolved. Here, we propose solutions to the existing problems and forecast the future trends of WSE.

(1) Ameliorate the performance of WSE. WSEs facilitate the formation of an anion-derived inorganic-rich electrode/electrolyte interphase. However, too weak solvation capability can hinder ion migration in the bulk electrolyte, leading to reduced ionic conductivity. Thus, solvents with extremely low solvation

© 2025 The Author(s). Advanced Energy Materials published by Wiley-VCH GmbH

16146840, 0, Downloaded from https://advanced.onlinelibrary.wiley.com/doi/10.1002/aenm.202501272 by Karlsruher Institut Für Technologie, Wiley Online Library on [13/05/2025]. See the Terms and Conditions (https://onlinelibrary.wiley.com/terms-and-conditions) on Wiley Online Library for rules of use; OA articles are governed by the applicable Creative Commons License

capability should be avoided. Additionally, it is necessary to consider the high-voltage performance and flame-retardant property of the electrolytes.

(2) Enhance the adaptability to a wide temperature range. Reported studies on WSE have predominantly focused on low temperature performance and fast charging, with less emphasis on their behavior under high temperature. However, operating at high temperature electrolytes are essential to promote the progress of battery technology for industrial and commercial value.

(3) Balance the overall compatibility within the battery. The development of high-performance electrolytes requires not only their intrinsic quality but also consideration of their compatibility with cathode and anode. This is because the electrolyte properties can significantly influence the formation and stability of both CEI/SEI layer, ion transport, and ultimately, the performance of the cell. Their interactions and compatibility are fundamental to achieve an outstanding electrochemical performance and safer battery operation.

(4) Reducing reliance on fluorinated solvents. The development of non-flammable WSEs has traditionally been reliant on high fluorine content. Although fluorinated solvents are effective in reducing flammability, they present challenges including high cost, environmental concerns, and poor biodegradability, especially for fully or extensively fluorinated derivatives. Therefore, developing low-fluorine or fluorine-free WSE should be considered in the selection of WSS. An alternative approach focuses on the modification of organophosphorus compounds and the exploration of silicone-based solvents. Recent research indicates that phosphorus-containing and silicone-containing compounds are good for flame retardancy, however, the electrochemical performance requires further improvement.

(5) Excel in the use of artificial intelligence. Artificial intelligence (AI) has gained attention in recent years, and the traditional trial-and-error model is both time-consuming and labor-intensive for developing new electrolytes. AI, in conjunction with big data, serves as a platform to inform the design of novel electrolytes, offering efficient and cost-effective methods of material discovery. AI-based methods such as neural networks, gaussian process regression, and graph neural networks can "learn" the correlation between structure, dynamics, and interactions with data obtained from computation and experiments. This revolution necessitates robust multidisciplinary collaboration amalgamating the expertise of material science, computer science, chemistry, and physics to solve the complex ties of battery technology development. The successful synergy of these disciplines offers a path toward the production of next-generation electrolytes.

Acknowledgements

X.L. and F.L. contributed equally to this work. Project funded by the National Natural Science Foundation of China (52161039) and the Jiangxi Provincial Natural Science Foundation (20224BAB204011). The Talent Project of Double Thousands Plan in Jiangxi Province (jxsq2020101056). Jiangxi Province Key Laboratory of Lithium-ion Battery Materials and Application (2024SSY05202), Natural Science Foundation of Hubei Province (2024AFB084), China Postdoctoral Science Foundation (2024M752502), Jiangxi Province Graduate Student Innovation Special Fund (YC2024-S127). S.P. acknowledged the basic funding of the Helmholtz Association and the Austrian Institute of Technology.

Open access funding enabled and organized by Projekt DEAL.

Conflict of Interest

The authors declare no conflict of interest.

Keywords

anions, interphase, rechargeable batteries, solvation structure, weakly solvating electrolyte

Received: March 6, 2025
Revised: March 29, 2025
Published online:

[1] X. Chen, N. Sawut, K. Chen, H. Li, J. Zhang, Z. Wang, M. Yang, G. Tang, X. Ai, H. Yang, Y. Fang, Y. Cao, *Energy Environ. Sci.* **2023**, *16*, 4041.
[2] L. Suo, Y.-S. Hu, H. Li, M. Armand, L. Chen, *Nat. Commun.* **2013**, *4*, 1481.
[3] Z. Li, Y. X. Yao, S. Sun, C. B. Jin, N. Yao, C. Yan, Q. Zhang, *Angew. Chem., Int. Ed.* **2023**, *62*, 202303888.
[4] X.-L. Gao, X.-H. Liu, W.-L. Xie, L.-S. Zhang, S.-C. Yang, *Rare Met.* **2021**, *40*, 3038.
[5] X.-B. Cheng, R. Zhang, C.-Z. Zhao, Q. Zhang, *Chem. Rev.* **2017**, *117*, 10403.
[6] J. Wang, Y. Yamada, K. Sodeyama, C. H. Chiang, Y. Tateyama, A. Yamada, *Nat. Commun.* **2016**, *7*, 12032.
[7] W. Xue, Z. Shi, M. Huang, S. Feng, C. Wang, F. Wang, J. Lopez, B. Qiao, G. Xu, W. Zhang, Y. Dong, R. Gao, Y. Shao-Horn, J. A. Johnson, J. Li, *Energy Environ. Sci.* **2020**, *13*, 212.
[8] H. Adenusi, G. A. Chass, S. Passerini, K. V. Tian, G. Chen, *Adv. Energy Mater.* **2023**, *13*, 2203307.
[9] K. Xu, *Chem. Rev.* **2004**, *104*, 4303.
[10] L. Suo, O. Borodin, T. Gao, M. Olguin, J. Ho, X. Fan, C. Luo, C. Wang, K. Xu, *Science* **2015**, *350*, 938.
[11] S. Chen, J. Zheng, D. Mei, K. S. Han, M. H. Engelhard, W. Zhao, W. Xu, J. Liu, J. G. Zhang, *Adv. Mater.* **2018**, *30*, 1706102.
[12] X. Cao, X. Ren, L. Zou, M. H. Engelhard, W. Huang, H. Wang, B. E. Matthews, H. Lee, C. Niu, B. W. Arey, Y. Cui, C. Wang, J. Xiao, J. Liu, W. Xu, J.-G. Zhang, *Nat. Energy* **2019**, *4*, 796.
[13] Y. Yamada, K. Furukawa, K. Sodeyama, K. Kikuchi, M. Yaegashi, Y. Tateyama, A. Yamada, *J. Am. Chem. Soc.* **2014**, *136*, 5039.
[14] L. Suo, D. Oh, Y. Lin, Z. Zhuo, O. Borodin, T. Gao, F. Wang, A. Kushima, Z. Wang, H. C. Kim, Y. Qi, W. Yang, F. Pan, J. Li, K. Xu, C. Wang, *J. Am. Chem. Soc.* **2017**, *139*, 18670.
[15] X. Ren, S. Chen, H. Lee, D. Mei, M. H. Engelhard, S. D. Burton, W. Zhao, J. Zheng, Q. Li, M. S. Ding, M. Schroeder, J. Alvarado, K. Xu, Y. S. Meng, J. Liu, J.-G. Zhang, W. Xu, *Chem* **2018**, *4*, 1877.
[16] X. Gao, Y. Chen, L. Johnson, P. G. Bruce, *Nat. Mater.* **2016**, *15*, 918.
[17] L. Lutz, D. Alves Dalla Corte, M. Tang, E. Salager, M. Deschamps, A. Grimaud, L. Johnson, P. G. Bruce, J.-M. Tarascon, *Chem. Mater.* **2017**, *29*, 6066.
[18] Z. Liu, L. Ma, L. Guo, Z. Peng, *J. Phys. Chem. Lett.* **2018**, *9*, 5915.
[19] Y. X. Yao, X. Chen, C. Yan, X. Q. Zhang, W. L. Cai, J. Q. Huang, Q. Zhang, *Angew. Chem., Int. Ed.* **2020**, *60*, 4090.
[20] X. Zheng, Z. Gu, J. Fu, H. Wang, X. Ye, L. Huang, X. Liu, X. Wu, W. Luo, Y. Huang, *Energy Environ. Sci.* **2021**, *14*, 4936.
[21] L. Deng, K. Goh, F.-D. Yu, Y. Xia, Y.-S. Jiang, W. Ke, Y. Han, L.-F. Que, J. Zhou, Z.-B. Wang, *Energy Storage Mater.* **2022**, *44*, 82.

© 2025 The Author(s). Advanced Energy Materials published by Wiley-VCH GmbH

16146840, 0, Downloaded from https://advanced.onlinelibrary.wiley.com/doi/10.1002/aenm.202501272 by Karlsruher Institut Für Technologie, Wiley Online Library on [13/05/2025]. See the Terms and Conditions (https://onlinelibrary.wiley.com/terms-and-conditions) on Wiley Online Library for rules of use; OA articles are governed by the applicable Creative Commons License

[22] J. Li, Y. Hu, H. Xie, J. Peng, L. Fan, J. Zhou, B. Lu, *Angew. Chem., Int. Ed.* **2022**, *61*, 202214198.
[23] Y. Jin, P. M. L. Le, P. Gao, Y. Xu, B. Xiao, M. H. Engelhard, X. Cao, T. D. Vo, J. Hu, L. Zhong, B. E. Matthews, R. Yi, C. Wang, X. Li, J. Liu, J.-G. Zhang, *Nat. Energy* **2022**, *7*, 718.
[24] D. T. Boyle, S. C. Kim, S. T. Oyakhire, R. A. Vilá, Z. Huang, P. Sayavong, J. Qin, Z. Bao, Y. Cui, *J. Am. Chem. Soc.* **2022**, *144*, 20717.
[25] L. Fan, H. Xie, Y. Hu, Z. Caixiang, A. M. Rao, J. Zhou, B. Lu, *Energy Environ. Sci.* **2023**, *16*, 305.
[26] M. Mao, X. Ji, Q. Wang, Z. Lin, M. Li, T. Liu, C. Wang, Y.-S. Hu, H. Li, X. Huang, L. Chen, L. Suo, *Nat. Commun.* **2023**, *14*, 1082.
[27] X. Liu, X. Zheng, Y. Dai, B. Li, J. Wen, T. Zhao, W. Luo, *Adv. Mater.* **2023**, *35*, 2210243.
[28] X. Shi, J. Xie, J. Wang, S. Xie, Z. Yang, X. Lu, *Nat. Commun.* **2024**, *15*, 302.
[29] S. Zhao, F. Huang, *ACS Nano* **2024**, *18*, 1733.
[30] X. Chen, Y.-K. Bai, C.-Z. Zhao, X. Shen, Q. Zhang, *Angew. Chem., Int. Ed.* **2020**, *59*, 11192.
[31] Z. Yu, H. Wang, X. Kong, W. Huang, Y. Tsao, D. G. Mackanic, K. Wang, X. Wang, W. Huang, S. Choudhury, Y. Zheng, C. V. Amanchukwu, S. T. Hung, Y. Ma, E. G. Lomeli, J. Qin, Y. Cui, Z. Bao, *Nat. Energy* **2020**, *5*, 526.
[32] Y. Huang, R. Li, S. Weng, H. Zhang, C. Zhu, D. Lu, C. Sun, X. Huang, T. Deng, L. Fan, L. Chen, X. Wang, X. Fan, *Energy Environ. Sci.* **2022**, *15*, 4349.
[33] K. Xu, A. von Cresce, U. Lee, *Langmuir* **2010**, *26*, 11538.
[34] G. Song, Z. Yi, F. Su, L. Xie, Z. Wang, X.-X. Wei, G. Xu, C.-M. Chen, *ACS Energy Lett.* **2023**, *8*, 1336.
[35] Z. Tian, Y. Zou, G. Liu, Y. Wang, J. Yin, J. Ming, H. N. Alshareef, *Adv. Sci.* **2022**, *9*, 2201207.
[36] N. Yao, X. Chen, X. Shen, R. Zhang, Z. H. Fu, X. X. Ma, X. Q. Zhang, B. Q. Li, Q. Zhang, *Angew. Chem., Int. Ed.* **2021**, *60*, 21473.
[37] Y. Chen, Z. Yu, P. Rudnicki, H. Gong, Z. Huang, S. C. Kim, J.-C. Lai, X. Kong, J. Qin, Y. Cui, Z. Bao, *J. Am. Chem. Soc.* **2021**, *143*, 18703.
[38] *J. Phys. Org. Chem.* **2011**, *24*, 743.
[39] Z. Wang, B. Zhang, *Energy Mater. Devices* **2023**, *1*, 9370003.
[40] D. T. Boyle, X. Kong, A. Pei, P. E. Rudnicki, F. Shi, W. Huang, Z. Bao, J. Qin, Y. Cui, *ACS Energy Lett.* **2020**, *5*, 701.
[41] S. Weng, X. Zhang, G. Yang, S. Zhang, B. Ma, Q. Liu, Y. Liu, C. Peng, H. Chen, H. Yu, X. Fan, T. Cheng, L. Chen, Y. Li, Z. Wang, X. Wang, *Nat. Commun.* **2023**, *14*, 4474.
[42] H. Zeng, K. Yu, J. Li, M. Yuan, J. Wang, Q. Wang, A. Lai, Y. Jiang, X. Yan, G. Zhang, H. Xu, J. Wang, W. Huang, C. Wang, Y. Deng, S.-S. Chi, *ACS Nano* **2024**, *18*, 1969.
[43] T. Ma, Y. Ni, Q. Wang, W. Zhang, S. Jin, S. Zheng, X. Yang, Y. Hou, Z. Tao, J. Chen, *Angew. Chem., Int. Ed.* **2022**, *134*, 202207927.
[44] H.-J. Liang, M.-Y. Su, X.-X. Zhao, Z.-Y. Gu, J.-L. Yang, W. Guo, Z.-M. Liu, J.-P. Zhang, X.-L. Wu, *Sci. China: Chem.* **2023**, *66*, 1982.
[45] Z. Wang, Y. Wang, B. Li, J. C. Bouwer, K. Davey, J. Lu, Z. Guo, *Angew. Chem., Int. Ed.* **2022**, *61*, 202206682.
[46] P. Xiao, X. Yun, Y. Chen, X. Guo, P. Gao, G. Zhou, C. Zheng, *Chem. Soc. Rev.* **2023**, *52*, 5255.
[47] Z. Jiang, J. Mo, C. Li, H. Li, Q. Zhang, Z. Zeng, J. Xie, Y. Li, *Energy Environ. Mater.* **2022**, *6*, 12440.
[48] F. Cataldo, *Eur. Chem. Bull.* **2015**, *4*, 92.
[49] H. Chu, J. Jung, H. Noh, S. Yuk, J. Lee, J.-H. Lee, J. Baek, Y. Roh, H. Kwon, D. Choi, K. Sohn, Y. Kim, H.-T. Kim, *Adv. Energy Mater.* **2020**, *10*, 2000493.
[50] C. M. C. F. Z. L. H. H. Y. M. Guangxiang Zhang, *Prog. Chem.* **2023**, *35*, 1534.
[51] J. Xu, J. Zhang, T. P. Pollard, Q. Li, S. Tan, S. Hou, H. Wan, F. Chen, H. He, E. Hu, K. Xu, X.-Q. Yang, O. Borodin, C. Wang, *Nature* **2023**, *614*, 694.
[52] Y. Wu, Q. Hu, H. Liang, A. Wang, H. Xu, L. Wang, X. He, *Adv. Energy Mater.* **2023**, 2300259.
[53] X. Liang, Z. Wen, Y. Liu, M. Wu, J. Jin, H. Zhang, X. Wu, *J. Power Sources* **2011**, *196*, 9839.
[54] X. Min, C. Han, S. Zhang, J. Ma, N. Hu, J. Li, X. Du, B. Xie, H. J. Lin, C. Y. Kuo, C. T. Chen, Z. Hu, L. Qiao, Z. Cui, G. Xu, G. Cui, *Angew. Chem., Int. Ed.* **2023**, *62*, 202302664.
[55] M. S. Kim, Z. Zhang, J. Wang, S. T. Oyakhire, S. C. Kim, Z. Yu, Y. Chen, D. T. Boyle, Y. Ye, Z. Huang, W. Zhang, R. Xu, P. Sayavong, S. F. Bent, J. Qin, Z. Bao, Y. Cui, *ACS Nano* **2023**, *17*, 3168.
[56] E. Park, J. Park, K. Lee, Y. Zhao, T. Zhou, G. Park, M.-G. Jeong, M. Choi, D.-J. Yoo, H.-G. Jung, A. Coskun, J. W. Choi, *ACS Energy Lett.* **2022**, *8*, 179.
[57] S. Kim, J.-A. Lee, T. K. Lee, K. Baek, J. Kim, B. Kim, J. H. Byun, H.-W. Lee, S. J. Kang, J.-A. Choi, S.-Y. Lee, M.-H. Choi, J.-H. Lee, N.-S. Choi, *Energy Environ. Sci.* **2023**, *16*, 5108.
[58] Y. Liao, M. Zhou, L. Yuan, K. Huang, D. Wang, Y. Han, J. Meng, Y. Zhang, Z. Li, Y. Huang, *Adv. Energy Mater.* **2023**, *13*, 2301670.
[59] T. Ma, Y. Ni, D. Li, Z. Zha, S. Jin, W. Zhang, L. Jia, Q. Sun, W. Xie, Z. Tao, J. Chen, *Angew. Chem., Int. Ed.* **2023**, *62*, 202307459.
[60] Y. Wang, Z. Li, Y. Hou, Z. Hao, Q. Zhang, Y. Ni, Y. Lu, Z. Yan, K. Zhang, Q. Zhao, F. Li, J. Chen, *Chem. Soc. Rev.* **2023**, *52*, 2713.
[61] C.-C. Su, M. He, R. Amine, T. Rojas, L. Cheng, A. T. Ngo, K. Amine, *Energy Environ. Sci.* **2019**, *12*, 1249.
[62] T. Li, X.-Q. Zhang, P. Shi, Q. Zhang, *Joule* **2019**, *3*, 2647.
[63] S.-J. Park, J.-Y. Hwang, C. S. Yoon, H.-G. Jung, Y.-K. Sun, *ACS Appl. Mater. Interfaces* **2018**, *10*, 17985.
[64] W. Xue, M. Huang, Y. Li, Y. G. Zhu, R. Gao, X. Xiao, W. Zhang, S. Li, G. Xu, Y. Yu, P. Li, J. Lopez, D. Yu, Y. Dong, W. Fan, Z. Shi, R. Xiong, C.-J. Sun, I. Hwang, W.-K. Lee, Y. Shao-Horn, J. A. Johnson, J. Li, *Nat. Energy* **2021**, *6*, 495.
[65] Q. Wang, Z. Yao, C. Zhao, T. Verhallen, D. P. Tabor, M. Liu, F. Ooms, F. Kang, A. Aspuru-Guzik, Y.-S. Hu, M. Wagemaker, B. Li, *Nat. Commun.* **2020**, *11*, 4188.
[66] Z. Cao, X. Zheng, M. Zhou, T. Zhao, L. Lv, Y. Li, Z. Wang, W. Luo, H. Zheng, *ACS Energy Lett.* **2022**, *7*, 3581.
[67] W. Cai, Y. Deng, Z. Deng, Y. Jia, Z. Li, X. Zhang, C. Xu, X. Q. Zhang, Y. Zhang, Q. Zhang, *Adv. Energy Mater.* **2023**, *13*, 2301396.
[68] Y. Mo, G. Liu, Y. Yin, M. Tao, J. Chen, Y. Peng, Y. Wang, Y. Yang, C. Wang, X. Dong, Y. Xia, *Adv. Energy Mater.* **2023**, *13*, 2301285.
[69] D. J. Yoo, Q. Liu, O. Cohen, M. Kim, K. A. Persson, Z. Zhang, *Adv. Energy Mater.* **2023**, *13*, 2204182.
[70] J. Wu, T. Zhou, B. Zhong, Q. Wang, W. Liu, H. Zhou, *ACS Appl. Mater. Interfaces* **2022**, *14*, 27873.
[71] Y. Li, M. Liu, K. Wang, C. Li, Y. Lu, A. Choudhary, T. Ottley, D. Bedrov, L. Xing, W. Li, *Adv. Energy Mater.* **2023**, *13*, 2300918.
[72] Y. Lu, W. Zhang, S. Liu, Q. Cao, S. Yan, H. Liu, W. Hou, P. Zhou, X. Song, Y. Ou, Y. Li, K. Liu, *ACS Nano* **2023**,*17*, 9586.
[73] L. Luo, K. Chen, H. Chen, H. Li, R. Cao, X. Feng, W. Chen, Y. Fang, Y. Cao, *Adv. Mater.* **2024**, *36*, 2308881.
[74] J. Shi, C. Xu, J. Lai, Z. Li, Y. Zhang, Y. Liu, K. Ding, Y. P. Cai, R. Shang, Q. Zheng, *Angew. Chem., Int. Ed.* **2023**, *62*, 202218151.
[75] S. C. Kim, J. Wang, R. Xu, P. Zhang, Y. Chen, Z. Huang, Y. Yang, Z. Yu, S. T. Oyakhire, W. Zhang, L. C. Greenburg, M. S. Kim, D. T. Boyle, P. Sayavong, Y. Ye, J. Qin, Z. Bao, Y. Cui, *Nat. Energy* **2023**, *8*, 814.
[76] P. Xiao, Y. Zhao, Z. Piao, B. Li, G. Zhou, H.-M. Cheng, *Energy Environ. Sci.* **2022**, *15*, 2435.
[77] N. Yao, L. Yu, Z. H. Fu, X. Shen, T. Z. Hou, X. Liu, Y. C. Gao, R. Zhang, C. Z. Zhao, X. Chen, Q. Zhang, *Angew. Chem., Int. Ed.* **2023**, *62*, 202305331.
[78] J. Wu, S. Zhang, C. Yang, X. Zhang, M. Zhou, W. Liu, H. Zhou, *Energy Storage Mater.* **2023**, *63*, 103043.
[79] C. Yang, M. Zheng, R. Qu, H. Zhang, L. Yin, W. Hu, J. Han, J. Lu, Y. You, *Adv. Mater.* **2023**, *36*, 2307220.

© 2025 The Author(s). Advanced Energy Materials published by Wiley-VCH GmbH

16146840, 0, Downloaded from https://advanced.onlinelibrary.wiley.com/doi/10.1002/aenm.202501272 by Karlsruher Institut Für Technologie, Wiley Online Library on [13/05/2025]. See the Terms and Conditions (https://onlinelibrary.wiley.com/terms-and-conditions) on Wiley Online Library for rules of use; OA articles are governed by the applicable Creative Commons License

[80] Y. Gao, W. Li, B. Ou, S. Zhang, H. Wang, J. Hu, F. Kang, D. Zhai, *Adv. Funct. Mater.* **2023**, *33*, 2300954.
[81] L. Kong, Y. Li, W. Feng, *Electrochem. Energy Rev.* **2021**, *4*, 633.
[82] T. D. Pham, A. Bin Faheem, H. D. Nguyen, H. M. Oh, K.-K. Lee, *J. Mater. Chem. A* **2022**, *10*, 12035.
[83] J. Tan, J. Matz, P. Dong, J. Shen, M. Ye, *Adv. Energy Mater.* **2021**, *11*, 2100046.
[84] Y.-H. Tan, G.-X. Lu, J.-H. Zheng, F. Zhou, M. Chen, T. Ma, L.-L. Lu, Y.-H. Song, Y. Guan, J. Wang, Z. Liang, W.-S. Xu, Y. Zhang, X. Tao, H.-B. Yao, *Adv. Mater.* **2021**, *33*, 2102134.
[85] Y. Rao, X. Li, S. Zhao, P. Liu, F. Wu, X. Liu, N. Zhou, S. Fang, S. Passerini, *Nano Energy* **2024**, *123*, 109362.
[86] M. Yuan, I. Tanabe, J.-M. Bernard-Schaaf, Q.-Y. Shi, V. Schlegel, R. Schurhammer, P. A. Dowben, B. Doudin, L. Routaboul, P. Braunstein, *New J. Chem.* **2016**, *40*, 5782.
[87] T. D. Pham, K. K. Lee, *Small* **2021**, *17*, 2100133.
[88] T. D. Pham, A. Bin Faheem, J. Kim, H. M. Oh, K. K. Lee, *Small* **2022**, *18*, 2107492.
[89] J. B. Goodenough, Y. Kim, *Chem. Mater.* **2010**, *22*, 587.
[90] R. Xu, J.-F. Ding, X.-X. Ma, C. Yan, Y.-X. Yao, J.-Q. Huang, *Adv. Mater.* **2021**, *33*, 2105962.
[91] J. Zhang, Q. Li, Y. Zeng, Z. Tang, D. Sun, D. Huang, Y. Tang, H. Wang, *ACS Energy Lett.* **2023**, *8*, 1752.
[92] X. Peng, B. Liu, J. Chen, Q. Jian, Y. Li, T. Zhao, *ACS Energy Lett.* **2023**, *8*, 3586.
[93] Y. Zhao, T. Zhou, T. Ashirov, M. E. Kazzi, C. Cancellieri, L. P. H. Jeurgens, J. W. Choi, A. Coskun, *Nat. Commun.* **2022**, *13*, 2575.
[94] X. Cao, P. Gao, X. Ren, L. Zou, M. H. Engelhard, B. E. Matthews, J. Hu, C. Niu, D. Liu, B. W. Arey, C. Wang, J. Xiao, J. Liu, W. Xu, J.-G. Zhang, *Proc. Natl. Acad. Sci. USA* **2021**, *118*, 2020357118.
[95] C. Fang, J. Li, M. Zhang, Y. Zhang, F. Yang, J. Z. Lee, M.-H. Lee, J. Alvarado, M. A. Schroeder, Y. Yang, B. Lu, N. Williams, M. Ceja, L. Yang, M. Cai, J. Gu, K. Xu, X. Wang, Y. S. Meng, *Nature* **2019**, *572*, 511.
[96] Y.-G. Cho, M. Li, J. Holoubek, W. Li, Y. Yin, Y. S. Meng, Z. Chen, *ACS Energy Lett.* **2021**, *6*, 2016.
[97] T. Jaumann, J. Balach, U. Langklotz, V. Sauchuk, M. Fritsch, A. Michaelis, V. Teltevskij, D. Mikhailova, S. Oswald, M. Klose, G. Stephani, R. Hauser, J. Eckert, L. Giebeler, *Energy Storage Mater.* **2017**, *6*, 26.
[98] J. Yun, L. Zhang, Q. Qu, H. Liu, X. Zhang, M. Shen, H. Zheng, *Electrochim. Acta* **2015**, *167*, 151.
[99] Y. Yang, Z. Li, Y. Xu, Z. Yang, Y. Zhang, J. Wang, H. Xu, X. He, H. Zhao, *J. Power Sources* **2023**, *577*, 233261.
[100] J. Xu, X. Wang, B. Hu, J. Ding, Z. Zhang, S. Ge, *Batteries Supercaps* **2023**, *6*, 202200499.
[101] S. Lei, Z. Zeng, M. Liu, H. Zhang, S. Cheng, J. Xie, *Nano Energy* **2022**, *98*, 107265.
[102] X. Kong, Y. Kong, L. He, W. Zhang, Y. Song, S. Liu, Y. Zhao, *J. Power Sources* **2022**, *551*, 232211.
[103] D. Xia, E. P. Kamphaus, A. Hu, S. Hwang, L. Tao, S. Sainio, D. Nordlund, Y. Fu, H. Huang, L. Cheng, F. Lin, *ACS Energy Lett.* **2023**, *8*, 1379.
[104] E. Santos, W. Schmickler, *Angew. Chem., Int. Ed.* **2021**, *60*, 5876.
[105] A. Hagopian, M.-L. Doublet, J.-S. Filhol, *Energy Environ. Sci.* **2020**, *13*, 5186.
[106] D. F. Shriver, B. L. Papke, M. A. Ratner, R. Dupon, T. Wong, M. Brodwin, *Solid State Ionics* **1981**, *5*, 83.
[107] Q. Zhao, X. Liu, S. Stalin, K. Khan, L. A. Archer, *Nat. Energy* **2019**, *4*, 365.
[108] F. Wu, Z. Chen, S. Fang, W. Zuo, G.-T. Kim, S. Passerini, *Energy Storage Mater.* **2023**, *63*, 103062.
[109] P. Wen, Y. Liu, J. Mao, X. Liu, W. Li, Y. Ren, Y. Zhou, F. Shao, M. Chen, J. Lin, X. Lin, *J. Energy Chem.* **2023**, *79*, 340.
[110] A. Wang, L. Wang, Y. Wu, Y. He, D. Ren, Y. Song, B. Zhang, H. Xu, X. He, *Adv. Energy Mater.* **2023**, *13*, 2300626.
[111] J. Xu, V. Koverga, A. Phan, A. min Li, N. Zhang, M. Baek, C. Jayawardana, B. L. Lucht, A. T. Ngo, C. Wang, *Adv. Mater.* **2023**, *36*, 2306462.
[112] C. Yan, H. R. Li, X. Chen, X. Q. Zhang, X. B. Cheng, R. Xu, J. Q. Huang, Q. Zhang, *J. Am. Chem. Soc.* **2019**, *141*, 9422.
[113] J. G. Zhang, W. Xu, J. Xiao, X. Cao, J. Liu, *Chem. Rev.* **2020**, *120*, 13312.
[114] Z. Wang, Z. Sun, J. Li, Y. Shi, C. Sun, B. An, H.-M. Cheng, F. Li, *Chem. Soc. Rev.* **2021**, *50*, 3178.
[115] S. Lin, H. Hua, P. Lai, J. Zhao, *Adv. Energy Mater.* **2021**, *11*, 2101775.
[116] Y.-C. Gao, N. Yao, X. Chen, L. Yu, R. Zhang, Q. Zhang, *J. Am. Chem. Soc.* **2023**, *145*, 23764.
[117] P. Peljo, H. H. Girault, *Energy Environ. Sci.* **2018**, *11*, 2306.
[118] S. Fang, F. Wu, S. Zhao, M. Zarrabeitia, G.-T. Kim, J.-K. Kim, N. Zhou, S. Passerini, *Adv. Energy Mater.* **2023**, *13*, 2302577.
[119] D. Aurbach, E. Markevich, G. Salitra, *J. Am. Chem. Soc.* **2021**, *143*, 21161.
[120] B. Scharifker, G. Hills, *Electrochim. Acta* **1983**, *28*, 879.
[121] M. E. Hyde, R. G. Compton, *J. Electroanal. Chem.* **2003**, *549*, 1.
[122] A. Bewick, M. Fleischmann, H. R. Thirsk, *Trans. Faraday Soc.* **1962**, *58*, 2200.
[123] M. Fleischmann, H. R. Thirsk, *J. Electrochem. Soc.* **1963**, *110*, 688.
[124] M. L. Fleischmann, H. R. Thirsk, *Electrochim. Acta* **1964**, *9*, 757.
[125] A. Milchev, I. Krastev, *Electrochim. Acta* **2011**, *56*, 2399.
[126] Y.-X. Yao, J. Wan, N.-Y. Liang, C. Yan, R. Wen, Q. Zhang, *J. Am. Chem. Soc.* **2023**, *145*, 8001.
[127] E. Peled, D. Golodnitsky, G. Ardel, *J. Electrochem. Soc.* **1997**, *144*, L208.
[128] K. Lim, B. Fenk, J. Popovic, J. Maier, *ACS Appl. Mater. Interfaces* **2021**, *13*, 51767.
[129] C. Ma, F. Xu, T. Song, *ACS Appl. Mater. Interfaces* **2022**, *14*, 20197.
[130] Z. Zhang, Y. Li, R. Xu, W. Zhou, Y. Li, S. T. Oyakhire, Y. Wu, J. Xu, H. Wang, Z. Yu, D. T. Boyle, W. Huang, Y. Ye, H. Chen, J. Wan, Z. Bao, W. Chiu, Y. Cui, *Science* **2022**, *375*, 66.
[131] B. Jagger, M. Pasta, *Joule* **2023**, *7*, 2228.
[132] E. Peled, S. Menkin, *J. Electrochem. Soc.* **2017**, *164*, A1703.
[133] X. Shen, R. Zhang, X. Chen, X.-B. Cheng, X. Li, Q. Zhang, *Adv. Energy Mater.* **2020**, *10*, 1903645.
[134] J. Y. Liang, Y. Zhang, S. Xin, S. J. Tan, X. H. Meng, W. P. Wang, J. L. Shi, Z. B. Wang, F. Wang, L. J. Wan, Y. G. Guo, *Angew. Chem., Int. Ed.* **2023**, *62*, 202300384.
[135] J. Xu, X. Wang, N. Yuan, J. Ding, S. Qin, J. M. Razal, X. Wang, S. Ge, Y. Gogotsi, *Energy Storage Mater.* **2019**, *23*, 383.
[136] A. Gupta, A. Manthiram, *Adv. Energy Mater.* **2020**, *10*, 2001972.
[137] J. Holoubek, H. Liu, Z. Wu, Y. Yin, X. Xing, G. Cai, S. Yu, H. Zhou, T. A. Pascal, Z. Chen, P. Liu, *Nat. Energy* **2021**, *6*, 303.
[138] C.-Y. Wang, G. Zhang, S. Ge, T. Xu, Y. Ji, X.-G. Yang, Y. Leng, *Nature* **2016**, *529*, 515.
[139] X. Fan, X. Ji, L. Chen, J. Chen, T. Deng, F. Han, J. Yue, N. Piao, R. Wang, X. Zhou, X. Xiao, L. Chen, C. Wang, *Nat. Energy* **2019**, *4*, 882.
[140] X. Chen, N. Yao, B.-S. Zeng, Q. Zhang, *Fundam. Res.* **2021**, *1*, 393.
[141] J.-F. Ding, R. Xu, N. Yao, X. Chen, Y. Xiao, Y.-X. Yao, C. Yan, J. Xie, J.-Q. Huang, *Angew. Chem., Int. Ed.* **2021**, *60*, 11442.
[142] Y. X. Yao, X. Chen, C. Yan, X. Q. Zhang, W. L. Cai, J. Q. Huang, Q. Zhang, *Angew. Chem., Int. Ed. Engl.* **2021**, *60*, 4090.
[143] T. Gao, Y. Han, D. Fraggedakis, S. Das, T. Zhou, C.-N. Yeh, S. Xu, W. C. Chueh, J. Li, M. Z. Bazant, *Joule* **2021**, *5*, 393.
[144] W. Cai, C. Yan, Y.-X. Yao, L. Xu, R. Xu, L.-L. Jiang, J.-Q. Huang, Q. Zhang, *Small Struct.* **2020**, *1*, 2000010.
[145] W. Mei, L. Jiang, H. J. Zhou, J. Sun, Q. Wang, *J. Energy Chem.* **2022**, *74*, 446.

© 2025 The Author(s). Advanced Energy Materials published by Wiley-VCH GmbH

16146840, 0, Downloaded from https://advanced.onlinelibrary.wiley.com/doi/10.1002/aenm.202501272 by Karlsruher Institut Für Technologie, Wiley Online Library on [13/05/2025]. See the Terms and Conditions (https://onlinelibrary.wiley.com/terms-and-conditions) on Wiley Online Library for rules of use; OA articles are governed by the applicable Creative Commons License

[146] Y. Yang, Z. Fang, Y. Yin, Y. Cao, Y. Wang, X. Dong, Y. Xia, *Angew. Chem., Int. Ed.* **2022**, *134*, 202208345.
[147] X. Dong, Z. Guo, Z. Guo, Y. Wang, Y. Xia, *Joule* **2018**, *2*, 902.
[148] X. Zhang, L. Zou, Y. Xu, X. Cao, M. H. Engelhard, B. E. Matthews, L. Zhong, H. Wu, H. Jia, X. Ren, P. Gao, Z. Chen, Y. Qin, C. Kompella, B. W. Arey, J. Li, D. Wang, C. Wang, J.-G. Zhang, W. Xu, *Adv. Energy Mater.* **2020**, *10*, 2000368.
[149] B. Nan, L. Chen, N. D. Rodrigo, O. Borodin, N. Piao, J. Xia, T. Pollard, S. Hou, J. Zhang, X. Ji, J. Xu, X. Zhang, L. Ma, X. He, S. Liu, H. Wan, E. Hu, W. Zhang, K. Xu, X. Q. Yang, B. Lucht, C. Wang, *Angew. Chem., Int. Ed.* **2022**, *61*, 202205967.
[150] H. Cheng, X. Jin, S. Liu, T. Zhang, Z. Song, L. Wang, F. Hu, *J. Power Sources* **2023**, *567*, 232975.
[151] B. Hu, Y. Wang, X. Qian, W. Chen, G. Liang, J. Chen, J. Zhao, W. Li, T. Chen, J. Fu, *ACS Nano* **2023**, *17*, 12734.
[152] C. Xie, S. Liu, H. Wu, Q. Zhang, C. Hu, Z. Yang, H. Li, Y. Tang, H. Wang, *Sci. Bull.* **2023**, *68*, 1531.
[153] X. Cao, W. Xu, D. Zheng, F. Wang, Y. Wang, X. Shi, X. Lu, *Angew. Chem., Int. Ed.* **2024**, *63*, 202317302.
[154] Y. Shang, D. Kundu, *Joule* **2023**, *7*, 244.
[155] L. Yuan, J. Hao, C.-C. Kao, C. Wu, H.-K. Liu, S.-X. Dou, S.-Z. Qiao, *Energy Environ. Sci.* **2021**, *14*, 5669.
[156] B. Tang, L. Shan, S. Liang, J. Zhou, *Energy Environ. Sci.* **2019**, *12*, 3288.
[157] J. Wang, H. Hu, L. Jia, J. Zhang, Q. Zhuang, L. Li, Y. Zhang, D. Wang, Q. Guan, H. Hu, M. Liu, L. Zhan, H. Adenusi, S. Passerini, H. Lin, *InfoMat* **2024**, *6*, 12558.
[158] K. W. Nam, H. Kim, Y. Beldjoudi, T.-w. Kwon, D. J. Kim, J. F. Stoddart, *J. Am. Chem. Soc.* **2020**, *142*, 2541.
[159] C. Zhao, Q. Wang, Z. Yao, J. Wang, B. Sánchez-Lengeling, F. Ding, X. Qi, Y. Lu, X. Bai, B. Li, H. Li, A. Aspuru-Guzik, X. Huang, C. Delmas, M. Wagemaker, L. Chen, Y. S. Hu, *Science* **2020**, *370*, 708.
[160] C. Bao, B. Wang, P. Liu, H. Wu, Y. Zhou, D. Wang, H. Liu, S. Dou, *Adv. Funct. Mater.* **2020**, *30*, 2004891.
[161] S. Wang, H. Xu, W. Li, A. Dolocan, A. Manthiram, *J. Am. Chem. Soc.* **2017**, *140*, 250.
[162] M. Zhang, Y. Li, F. Wu, Z. Wang, Y. Bai, C. Wu, *J. Mater. Chem. A* **2021**, *9*, 10780.
[163] X. Zhou, Q. Zhang, Z. Zhu, Y. Cai, H. Li, F. Li, *Angew. Chem., Int. Ed.* **2022**, *61*, 202205045.
[164] Y. Zhao, L. Zhang, J. Liu, K. Adair, F. Zhao, Y. Sun, T. Wu, X. Bi, K. Amine, J. Lu, X. Sun, *Chem. Soc. Rev.* **2021**, *50*, 3889.
[165] Y. Zou, Z. Ma, G. Liu, Q. Li, D. Yin, X. Shi, Z. Cao, Z. Tian, H. Kim, Y. Guo, C. Sun, L. Cavallo, L. Wang, H. N. Alshareef, Y. K. Sun, J. Ming, *Angew. Chem., Int. Ed.* **2023**, *62*, 202216189.
[166] H. Wang, C. Zhu, J. Liu, S. Qi, M. Wu, J. Huang, D. Wu, J. Ma, *Angew. Chem., Int. Ed.* **2022**, *61*, 202208506.
[167] J. Zhou, Y. Wang, J. Wang, Y. Liu, Y. Li, L. Cheng, Y. Ding, S. Dong, Q. Zhu, M. Tang, Y. Wang, Y. Bi, R. Sun, Z. Wang, H. Wang, *Energy Storage Mater.* **2022**, *50*, 47.
[168] Y.-Q. Zheng, M.-Y. Sun, F.-D. Yu, L. Deng, Y. Xia, Y.-S. Jiang, L.-F. Que, L. Zhao, Z.-B. Wang, *Nano Energy* **2022**, *102*, 107693.
[169] D. A. Rakov, F. Chen, S. A. Ferdousi, H. Li, T. Pathirana, A. N. Simonov, P. C. Howlett, R. Atkin, M. Forsyth, *Nat. Mater.* **2020**, *19*, 1096.
[170] K. Li, J. Zhang, D. Lin, D.-W. Wang, B. Li, W. Lv, S. Sun, Y.-B. He, F. Kang, Q.-H. Yang, L. Zhou, T.-Y. Zhang, *Nat. Commun.* **2019**, *10*, 725.
[171] L. Wu, M. Gu, Y. Feng, S. Chen, L. Fan, X. Yu, K. Guo, J. Zhou, B. Lu, *Adv. Funct. Mater.* **2022**, *32*, 2109893.
[172] L. Fan, Y. Hu, A. M. Rao, J. Zhou, Z. Hou, C. Wang, B. Lu, *Small Methods* **2021**, *5*, 2101131.
[173] W. Luo, Y. Feng, D. Shen, J. Zhou, C. Gao, B. Lu, *ACS Appl. Mater. Interfaces* **2022**, *14*, 16379.
[174] M. Zarrabeitia, J. Carretero-González, M. Leskes, H. Adenusi, B. Iliev, T. J. S. Schubert, S. Passerini, E. Castillo-Martinez, *Energy Mater.* **2023**, *3*, 300046.
[175] Z. Yu, Q. Liu, C. Chen, Y. Zhu, B. Zhang, *J. Power Sources* **2023**, *557*, 232550.
[176] M. Tang, S. Dong, J. Wang, L. Cheng, Q. Zhu, Y. Li, X. Yang, L. Guo, H. Wang, *Nat. Commun.* **2023**, *14*, 6006.
[177] L. Li, L. Liu, Z. Hu, Y. Lu, Q. Liu, S. Jin, Q. Zhang, S. Zhao, S. L. Chou, *Angew. Chem., Int. Ed.* **2020**, *59*, 12917.
[178] Y. Xu, T. Ding, D. Sun, X. Ji, X. Zhou, *Adv. Funct. Mater.* **2022**, *33*, 2211290.
[179] L. Xue, Y. Li, H. Gao, W. Zhou, X. Lü, W. Kaveevivitchai, A. Manthiram, J. B. Goodenough, *J. Am. Chem. Soc.* **2017**, *139*, 2164.
[180] L. Deng, J. Qu, X. Niu, J. Liu, J. Zhang, Y. Hong, M. Feng, J. Wang, M. Hu, L. Zeng, Q. Zhang, L. Guo, Y. Zhu, *Nat. Commun.* **2021**, *12*, 2167.
[181] S. Liu, J. Mao, L. Zhang, W. K. Pang, A. Du, Z. Guo, *Adv. Mater.* **2020**, *33*, 2006313.
[182] Y. Hu, L. Fan, A. M. Rao, W. Yu, C. Zhuoma, Y. Feng, Z. Qin, J. Zhou, B. Lu, *Natl. Sci. Rev.* **2022**, *9*, nwac134.
[183] Z. Jian, W. Luo, X. Ji, *J. Am. Chem. Soc.* **2015**, *137*, 11566.
[184] S. Alvin, H. S. Cahyadi, J. Hwang, W. Chang, S. K. Kwak, J. Kim, *Adv. Energy Mater.* **2020**, *10*, 2000283.
[185] J. Yang, Z. Ju, Y. Jiang, Z. Xing, B. Xi, J. Feng, S. Xiong, *Adv. Mater.* **2017**, *30*, 1700104.
[186] F. Ming, Y. Zhu, G. Huang, A.-H. Emwas, H. Liang, Y. Cui, H. N. Alshareef, *J. Am. Chem. Soc.* **2022**, *144*, 7160.
[187] N. Xiao, W. D. McCulloch, Y. Wu, *J. Am. Chem. Soc.* **2017**, *139*, 9475.

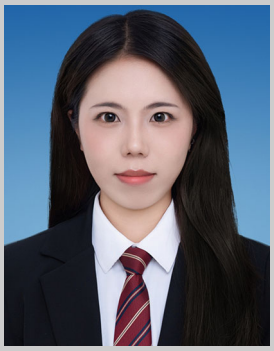

Xue Li received her bachelor's degree from Southwest University of Science and Technology in 2022 and is now pursuing her master's degree in the School of Physics and Materials Science at Nanchang University. Her main research interests are the optimization of functional electrolyte and anode interface stability for lithium metal batteries.

© 2025 The Author(s). Advanced Energy Materials published by Wiley-VCH GmbH

16146840, 0, Downloaded from https://advanced.onlinelibrary.wiley.com/doi/10.1002/aenm.202501272 by Karlsruher Institut Für Technologie, Wiley Online Library on [13/05/2025]. See the Terms and Conditions (https://onlinelibrary.wiley.com/terms-and-conditions) on Wiley Online Library for rules of use; OA articles are governed by the applicable Creative Commons License

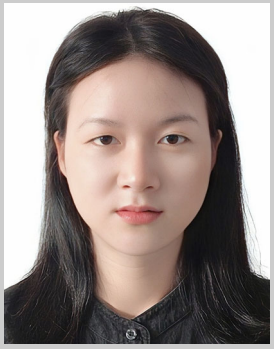

Fei Luo earned her bachelor's degree from Jingdezhen Ceramic University in 2023 and is pursuing her master's degree in the School of Physics and Materials Science at Nanchang University. Her research focuses on lithium metal battery electrolytes for wide temperature ranges and high-voltage applications.

Naigen Zhou is a Professor at Nanchang University, a leading academic and technical figure in Jiangxi Province (leading talent). He worked as a postdoctoral researcher at Brown University in the United States in 2008-2009. His main research involves computational simulation and experimental studies on new energy materials and devices for lithium batteries. Currently, he is the leader of the subdiscipline of new energy materials and devices in the "first-class discipline" of materials science and engineering at Nanchang University, as well as the leader of the energy materials and devices team at the School of Physics and Materials Science at Nanchang University.

Henry Adenusi is an Assistant Professor of experimental physics at Marche Polytechnic University with a research focus on energy storage systems, ionic liquids, and liquid crystals. He completed his Postdoctoral Fellowship at the University of Hong Kong – Hong Kong Quantum AI Lab, a joint center with the California Institute of Technology, investigating next-generation energy storage materials. Also, he received his PhD from Sapienza University of Rome, a recipient of the 'Vito Volterra' International PhD Fellowship.

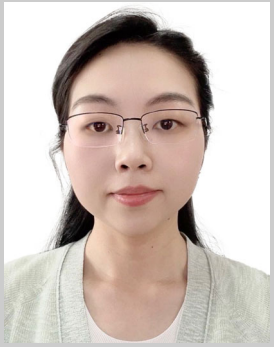

Shan Fang is a professor at the School of Physics and Materials Science of Nanchang University. She received her Ph.D. at Nanjing University of Aeronautics and Astronautics (NUAA) in 2018, then worked as a staff scientist at Karlsruhe Institute of Technology (KIT) and Helmholtz Institute Ulm (HIU) from 2018 to 2020. Her research focuses on key materials for high-energy-density advanced batteries.

© 2025 The Author(s). Advanced Energy Materials published by Wiley-VCH GmbH

16146840, 0, Downloaded from https://advanced.onlinelibrary.wiley.com/doi/10.1002/aenm.202501272 by Karlsruher Institut Für Technologie, Wiley Online Library on [13/05/2025]. See the Terms and Conditions (https://onlinelibrary.wiley.com/terms-and-conditions) on Wiley Online Library for rules of use; OA articles are governed by the applicable Creative Commons License

Fanglin Wu received his bachelor's degree from Sichuan University in 2015 and his master's degree from Wuhan University of Technology in 2017. Later, he completed his Ph.D. degree at the Karlsruhe Institute of Technology (KIT) under the supervision of Prof. Dr. Stefano Passerini and continued working at KIT as a post-doctoral researcher. Currently, he is working at Wuhan University of Technology; the research is focusing on high-safety ionic liquid-based electrolytes and solid-state electrolytes for high-specific-energy lithium metal batteries.

Stefano Passerini is a professor at the Center for Transport Technologies of the Austrian Institute of Technology and a Distinguished Senior Fellow at Karlsruhe Institute of Technology. His research focuses on the basic understanding and development of materials for high-energy batteries and supercapacitors, with the goal of creating sustainable energy storage systems from environmentally friendly and available materials and processes.

© 2025 The Author(s). Advanced Energy Materials published by Wiley-VCH GmbH

16146840, 0, Downloaded from https://advanced.onlinelibrary.wiley.com/doi/10.1002/aenm.202501272 by Karlsruher Institut Für Technologie, Wiley Online Library on [13/05/2025]. See the Terms and Conditions (https://onlinelibrary.wiley.com/terms-and-conditions) on Wiley Online Library for rules of use; OA articles are governed by the applicable Creative Commons License